Princeton Plasma Physics Laboratory

PPPL- 4999

PPPL- 4999

Effect of Deuterium Gas Puff On The Edge Plasma In NSTX

S.J. Zweben, et. al.

FEBRUARY, 2014

PPPL PRINCETON PLASMA PHYSICS LABORATORY

Prepared for the U.S. Department of Energy under Contract DE-AC02-09CH11466.

Princeton Plasma Physics Laboratory
Report Disclaimers

Full Legal Disclaimer

Trademark Disclaimer

PPPL Report Availability

Princeton Plasma Physics Laboratory:

http://www.pppl.gov/techreports.cfm

Office of Scientific and Technical Information (OSTI):

http://www.osti.gov/bridge

Related Links:

U.S. Department of Energy

Office of Scientific and Technical Information

Fusion Links

Effect of a deuterium gas puff on the edge plasma in NSTX

S.J. Zweben, D.P. Stotler, R.E. Bell, W.M. Davis, S.M. Kaye, E.T. Meier[1], T. Munsat[2], B.P. LeBlanc, R.J. Maqueda[3], Y. Ren, Y. Sechrest[2], D.R. Smith[4], and V. Soukhanovskii[1]

Princeton Plasma Physics Laboratory, Princeton NJ 08540
[1] Lawrence Livermore National Laboratory, Livermore, CA 94550
[2] University of Colorado, Boulder CO 80309
[3] X Science LLC, Princeton NJ 08540
[4] University of Wisconsin, Madison WI 53706

ABSTRACT

This paper describes a detailed examination of the effects of a relatively small pulsed deuterium gas puff on the edge plasma and edge turbulence in NSTX. This gas puff caused little or no change in the line-averaged plasma density or total stored energy, or in the edge density and electron temperature up to the time of the peak of the gas puff. The radial profile of the Dα light emission and the edge turbulence within this gas puff did not vary significantly over its rise and fall, implying that these gas puffs did not significantly perturb the local edge plasma or edge turbulence. These measurements are compared with modeling by DEGAS 2, UEDGE, and with simplified estimates for the expected effects of this gas puff.

1. Introduction

Almost all tokamak experiments use hydrogen or deuterium gas puffing to fuel the plasma and to increase the plasma density. These neutral molecular gases are puffed into the chamber through fast-acting valves at the vacuum vessel wall, and usually only small fraction of this incoming gas enters the plasma edge and becomes ionized. The location and strength of these neutral gas sources is generally not well documented, and relatively little is understood about the effect of these gas puffs on the plasma.

The goal of this paper is to describe the effects of a deuterium gas puff on the edge plasma in NSTX, which is a low aspect ratio tokamak [1]. There are two different motivations for this study. The first is to determine whether this specific deuterium gas puff used the NSTX gas puff imaging (GPI) diagnostic has any significant perturbing effects on the edge turbulence which it is designed to measure. The second motivation is to better understand the response of the plasma edge to the deuterium fueling puffs, using these GPI gas puffs as test cases.

The effect of a gas puff can be quite complex and difficult to predict from first principles, since it depends on the particle and energy transport mechanisms in the edge plasma, which are not well understood. In general, any edge particle source will increase the density where its ionization occurs, and the edge temperature nearby will decrease due energy loss from ionization, radiation and charge exchange from the neutrals. The response of the plasma to these sources and sinks will depend on both the parallel and the cross-field transport.

The GPI diagnostic on NSTX measures the 2-D structure and motion of edge turbulence by viewing the visible light emitted by a dedicated deuterium (or helium) gas puff introduced into the plasma edge [2-4]. Ideally, this gas puff should introduce as little gas as possible to minimize perturbations to the local edge plasma and/or the edge turbulence. The earliest NSTX deuterium GPI results showed no changes in the turbulence characteristics vs. time over a factor of ~x5 in the helium gas puff influx rate with a total gas puff of ~1 Torr-liter (6.6×10^{19} D atoms or 3.6×10^{19} He atoms) [2], and later NSTX GPI results with similar gas puff levels of helium or deuterium produced no significant change in either reflectometer or probe measurements of edge turbulence [3]. Recently the GPI deuterium gas influx rate has been increased to ~3-6 Torr-liters [4], partly due to the x3 faster framing rate and smaller exposure time of the GPI camera, and partly due to a gradual radiation darkening of the fiber optic bundle carrying the images. The present paper reassesses the GPI puff effects at this higher gas influx rate.

The edge effects of gas puffs have been discussed in the context of several previous experiments. In the TJ-II stellarator [5], the edge Dα light was increased by deuterium gas puffing by a factor of $\leq$3.5 with no systematic changes in the edge turbulence. In PBX-M [5], helium gas puffing correlated with a $\leq$2 increase in the relative edge turbulence level, but only when the edge electron temperature decreased by a factor of two due to the helium. In ASDEX Upgrade [6] and JET [7], deuterium puffs of ~$0.5\text{-}1.0 \times 10^{22}$ atoms/sec (similar to the present experiment) were recently used to

improve the ICRH and LH coupling (respectively), but no measurements of edge turbulence were reported.

Gas puff effects were also studied in non-diverted hydrogen Ohmic discharges in the small ADITYA tokamak [8,9]. Several effects on edge fluctuations and transport were observed, including a flattening of the edge floating potential profile, a decrease in edge density gradient, a reduction in edge floating potential fluctuations, and a x2 increase in global confinement time [8]. These gas puffs also reduced the edge poloidal flow speed, and caused reversal in the toroidal flow speed due to the local edge particle source [9]. Gas puff effects in non-diverted hydrogen Ohmic discharges were also studied on the small STOR-M tokamak [10], where the line-averaged density was doubled by these gas puff, but the loop voltage decreased, indicating an increase in the core electron temperature and global confinement. The SOL density increased and electron temperature decreased ~1-3 msec after the puff, along with a reduction in the floating potential fluctuations, as in ADITYA [8].

The previous results most closely related to the present paper were obtained using GPI diagnostics on other tokamaks. Deuterium gas puff rates of $\sim 10^{19}$-10^{20} atoms/sec were used in early GPI experiments on Alcator C-Mod [11], and no significant change in the fluctuations in a Langmuir probe at the same minor radius as the GPI gas cloud were observed. Helium gas puff rates up to $\sim 10^{21}$ atoms/sec were recently used for GPI in Alcator C-Mod [12], and estimates of the possible perturbing effects of these puffs were made, although edge plasma variations were not reported. Helium puffing was also used in the dual GPI diagnostic in the EAST tokamak [13] with an average puff rate (per GPI view) of $\sim 2 \times 10^{20}$ atoms/sec over 250 msec, with an acceptable level of perturbation. In the TEXTOR tokamak a deuterium GPI system was operated with a low divergence gas nozzle [14], and measurements of edge density and temperature profiles in the edge and SOL showed no significant change with or without the puff up to gas influx rates $\sim 4.6 \times 10^{20}$ atoms/sec, although a slight decrease in ion saturation current fluctuations at the outer midplane was observed by a Langmuir probe at the higher puff rates.

The response of the edge plasma to supersonic gas injection was also measured and modeled in Tore-Supra [15]. The amount of deuterium gas puffed was $1\text{-}5 \times 10^{20}$ atoms in 2-4 msec, i.e. up to $\sim 10^{23}$ atoms/sec. Measurements made with Langmuir probes 2 cm outside the separatrix showed a large increase in the SOL plasma density and parallel Mach speed, and a factor of two decrease in the SOL electron temperature just after the gas puff. The local effects of strong deuterium gas fueling were also measured in TEXTOR during radiative improved (RI) modes operation [16]. The deuterium injection rate varied between 10^{20}-3×10^{21} atoms/sec, and measurements were made of the deuterium atomic and molecular spectra in the gas cloud to infer the local electron temperature, which decreased significantly at the highest gas puff rates.

Other previous tokamak experiments have studied the interaction between gas puffing and the L-H transition. A strong gas puff was observed to rapidly increase the edge density and trigger an L-H transition in non-diverted Ohmic plasmas in the Tuman-3 tokamak [17]. In the low-aspect ratio tokamaks MAST [18] and NSTX [19], it was

found that high-field side (i.e. inner wall) gas fueling at a rate of ~$3x10^{21}$ D atoms/sec facilitates the L-H transition, compared with the usual low-field-side gas fueling.

Gas puffing experiments have been of more general interest for many years in the study of particle confinement in tokamaks; for example, in PLT [20], TEXT [21], TFTR [22], DIII-D [23], and recently in T-10 [24]. In most of these experiments the focus was on core particle transport, and there were relatively few measurements of the local effects of these gas puffs on the edge plasma, although a possible effect of the small gas puffs in T-10 on the edge temperature was noted in Ref. [24].

There have been several theoretical analyses of the effects of edge neutrals on poloidal ExB plasma flow in the context of L-H transition studies. Large deuterium gas puff rates in DIII-D of ~10^{22} atoms/sec for ~0.5 sec increased the neutral density and line-averaged plasma density significantly [25], and a correlation was found between the edge neutral density and the L-H power threshold. The effect of neutrals on various edge instabilities was analyzed in [26], and poloidally localized refueling was proposed as a method to control edge plasma rotation through the charge exchange (CX) transfer of momentum [27]. The neoclassical theory of toroidal rotation in the presence of asymmetric gas puffing in the tokamak edge was discussed in [28]. Finally, recent simulations of L-H transitions also showed a sensitivity to the edge particle injection rate *via* changes in the edge temperature [29].

There has been an extensive series of theoretical analyses by Tokar *et al* of the local effects of deuterium or impurity gas puffs on the edge thermal stability and tokamak density limit [16, 30-33]. The most recent analysis [33] treats this problem by solving a non-stationary, two-dimensional heat conduction equation numerically, and includes a heat flux limit and the density response to edge cooling. Two-dimensional numerical modeling of the ionization of gas puffed atoms in the edge plasma has also been included in the comprehensive EDGE2D [34] and UEDGE codes [35], although the 3-D nature of a localized gas puff is beyond the scope of these codes.

Finally, we mention other edge particle sources in tokamaks: supersonic gas nozzles in NSTX can inject up to ~10^{22} atoms/sec of deuterium to improve the fueling efficiency [36], and small deuterium pellets have been injected with 2-$6x10^{21}$ atoms/sec to control ELMS in DIII-D [37]. Impurity gas puffing of nitrogen at a level of ~10^{22} electrons/sec has been used to increase edge radiation and reduce the SOL temperature e.g. in JET [38], and massive impurity gas injection has been used on DIII-D [39] and Alcator C-Mod [40] to terminate the discharge to mitigate disruptions.

The outline of this paper is as follows: Sec. 2 describes the experimental results, Sec. 3 describes the modeling and interpretation of these results, and Sec. 4 includes a discussion these results.

2. Experimental results

Section 2.1 describes the plasma parameters and gas puff, Sec. 2.2 describes the Thomson scattering measurements, and Sec. 2.3 describes GPI profile data, which give the most direct measurement of the local effects of the GPI gas puff. Section 2.4 describes the GPI turbulence measurements, Sec. 2.5 describes other diagnostic data, and Section 2.6 describes the (absence of) effects of the puff on the L-H transition and ELMs.

2.1 Plasma parameters and deuterium gas puffs

Table 1 lists the plasma parameters for the 27 NSTX discharges from 2010 used for this paper. The plasma currents ranged from 0.7-1.1 MA, the toroidal fields from 3.6-5.4 kG, and the applied neutral beam injection (NBI) or radio frequency (RF) power from 0-6 MW. These are low aspect ratio plasmas with major radius R~85 cm and minor radius a~65 cm with a diverted, lower-single-null shape with an elongation of ~2.2.

The shots in Table 1 were chosen to have constant global parameters within ±100 msec of the peak of the GPI puff time in Table 1, i.e. constant plasma current, B field, plasma shape, and NBI or RF power. Also these shots were selected to have no large transient events during the times of interest, e.g. no L-H transitions or large ELMs, and to have GPI data taken with the fastest possible rate for turbulence analysis (400,000 frames/sec). Only the first two groups in Table 1 had "no puff" comparison shots with similar conditions, although all shots include a "pre-puff" period for comparison within the shot. All of these plasmas were all far from the Greenwald density limit, e.g. $n/n_G \sim 0.5$ for #138846 @ 0.6 sec.

The deuterium gas puff hardware is the same as used previously for the gas puff imaging (GPI) diagnostic on NSTX [2-4], as shown in Fig. 1. The GPI puff enters the plasma through a 30 cm long gas manifold located near the outer wall of the vessel and centered about 20 cm above the outer midplane, as previously described in [4]. The gas exits the manifold through 30 holes each of 1 mm diameter spaced 1 cm apart facing the plasma. The manifold holes were ~2 cm radially behind the shadow of the RF antenna structure, which formed the outer midplane limiter in NSTX, and the radial distance of the magnetic separatrix from this limiter was typically ~5-10 cm (see Table 1). The manifold was oriented perpendicular to the local edge B field direction, which was typically at an angle ~40º with respect to horizontal in NSTX. The deuterium gas was stored in a room-temperature plenum, and a piezoelectric valve was triggered once per shot to fill the manifold and puff the gas into the plasma. The gas puffed into these plasmas ranged from ~3-6 Torr-liters of deuterium per shot. No attempt was made to spatially collimate this gas puff or to create a supersonic gas nozzle.

Figure 2(a) shows the time dependence of the plasma current (top), NBI power, line averaged electron density measured by Thomson scattering, and the total $D\alpha$ light emission from the GPI puff for the first group of shots of Table 1. Shot 138843 has no GPI puff, while the three successive shots have very similar GPI puffs of ~5.5 Torr-liters.

For these cases the GPI gas valve was pulsed at 0.580 sec for 30 msec, the Dα light emission from this puff began to increase at 0.593 sec, and the GPI Dα signal level peaked at 0.613 sec at a level ≥20 times the background Dα before the GPI puff. About 20% of the time-integrated Dα light emission from the GPI puff occurred by the time of its peak, after which the Dα light decayed with an e-folding time of ~50 msec due to draining of the gas manifold. About 80% of the total gas puff Dα light emission occurred by 67 msec after the peak of the Dα light emission.

Table 2 summarizes the gas puff parameters for a typical shot of Fig. 2(a). The total gas puff was 5.7 Torr-liters or 3.8 x 10^{20} deuterium atoms, with a peak neutral influx rate of ~$6.6x10^{21}$ atoms/sec and an average neutral influx rate over the first 100 msec of ~$3.2x10^{21}$ atoms/sec. The total number of neutrals puffed into the chamber by the time of the peak of the puff (0.613 sec) is $7.6x10^{19}$ atoms, and by 67 msec after the peak this is 4x larger, i.e. ~$3x10^{20}$ atoms. The total number of electrons inside the confined plasma just before the GPI puff was N_{tot}~$6x10^{20}$ electrons, so the gas puff had ~13% of the plasma electron content by the time of the peak of the gas puff, and ~50% by 67 msec after the peak of the puff. However, only a small fraction (~25%) of the neutrals coming from the manifold will be ionized in the main plasma, and these ions will quickly be lost by edge particle diffusion, so the expected global rise in density is ≤3% by the time of the peak of the puff. Particle balance estimates are discussed further in Sec. 3.

The absolute level of Dα light emission from this puff was previously evaluated using the GPI imaging system, and was consistent to within ~35% with the expected Dα light level for this gas puff based on pressure gauge calibrations and DEGAS 2 simulations, as described in Ref. [4]. Other deuterium gas sources for the discharge in Fig. 2(a) at the time of the GPI puff were: ~1.3-$1.9x10^{21}$ D/sec from the center stack gas injector (slowly decaying from a puff started earlier in the shot), ~$4x10^{20}$ D/sec from NBI (according to TRANSP), and ~$1.2x10^{22}$ D/sec recycled from the outer divertor target and ~$1.4x10^{22}$ D/sec recycled from the inner divertor target (according to UEDGE). Thus the peak GPI gas puff rate was ≤25% of the total neutral deuterium influx rate at this time, most of which came from recycling in the divertor region.

There is no visible effect of these GPI gas puffs on the time evolution of the line-averaged electron density in NSTX in Fig. 2(a). This is perhaps because the density is continuously rising vs. time even without the puff, since there is not enough wall pumping to maintain a steady state density [41]. Figure 2(b) shows the total plasma stored energy before vs. after the GPI puff for all the shots in the database of Table 1, based on the energy inferred from the EFIT magnetic equilibria. The horizontal axis shows the stored energy just before the start of the GPI puff, and the vertical axis shows the stored energy at the peak of the GPI puff and 30 msec and 60 msec later. The black points show the 'no puff' comparison shots for the first two groups in Table 1, and the black line is drawn at unity slope. The ratio of the stored energy during the GPI puff to just before the GPI puff was 1.1±0.2 at the peak of the puff, 1.2±0.3 at 30 msec after the peak, and 1.2±0.3 at 60 msec after the peak. Thus the GPI gas puff does not significantly change the total stored energy, and also does not affect the magnetic separatrix location, the radiated power, or other parameters, as discussed in Sec. 2.5.

2.2 Thomson scattering data

The Thomson scattering diagnostic measures the electron density and temperature profiles on the NSTX midplane ~150º degrees toroidally from the GPI puff, and also far from the magnetic field lines going through the puff. These measurement channels have a radial separation of ~2 cm, a time separation of 16.6 msec, with error bars based on the photon statistics.

Figure 3 shows a comparison of the Thomson profiles for two of the shots of Fig. 2(a), without a puff in Fig. 3(a) and with a GPI puff in Fig. 3(b), along with the line-integrated density, central electron temperature, and GPI $D\alpha$ signals. The line-integrated density and central electron temperature are not significantly affected by the gas puff, but after the peak of the puff there does seem to be a change in the edge temperature, but not in the edge density.

This change in edge parameters after the peak of the GPI puff is illustrated more clearly in Figs. 4 and 5. These figures show the time and spatial dependence of the Thomson edge T_e and n_e data for the four shots of Fig. 2(a), with one shot without a gas puff (black) and the other three with a gas puff (green, red, and blue). The separatrix position is constant within 0.2 cm from shot-to-shot, as listed in Table 1. All of these shots are H-mode plasmas.

Figure 4 shows little or no systematic change in either T_e or n_e with respect to the "no puff" comparison shot up to the time of the peak of the GPI puff, indicated by the vertical black line. However, in the shots with a gas puff there was a ~20-30±10% decrease in T_e by ~50-100 msec after the peak of the GPI puff at 7.4 cm, 5.4 cm and 3.8 cm inside the separatrix in Figs. 4(a), (b), and (c), when compared with the "no-puff" shot. There were also ~10-15% increases in n_e at 5.3 cm and 3.8 cm inside the separatrix by ~50 msec after the peak of the puff, but little or no increases at 7.4 cm inside the separatrix. The measurements at 1.4 cm inside the separatrix in Fig. 4(d) are dominated by random-looking fluctuations. The second group of shots in Table 1 shows qualitatively similar trends to those in Figs. 4.

Figure 5 shows the radial profiles of this T_e and n_e data in the edge region up to ~ 10 cm inside the separatrix for four different times for the same set of shots as for Fig. 4. Also shown are the GPI radial profiles for these times (black dots), mapped along flux surfaces to the outer midplane where the Thomson data is taken. The horizontal axis is the distance from the outer midplane separatrix, and the H-mode 'pedestal' in density occurs ~2-4 cm inside the separatrix. The profiles in Fig. 5(a) at 31 msec before the peak of the GPI puff are similar for all four shots. The profiles in Fig. 5(b) taken ~2 msec after the peak of the GPI puff show little or no systematic change, but the profiles below at 35 msec and 69 msec after the peak of the GPI puff in Figs. 5(c) and 5(d) show a clear decreases in $T_{e\ from}$ ~ 3-10 cm inside the separatrix. The data in the SOL does not show consistent trends within the error bars.

To help clarify these trends, Fig. 6 shows all the points in Fig. 5 for the first two groups of shots in Table 1, but sorted by time with respect to the peak of the gas puff.

The electron temperatures are plotted in Figs. 6(a) and (on log scale) in 6(b), and the densities are plotted in Figs. 6(c) and (in log scale) in Fig. 6(d). The points from the shots with no GPI gas puff are marked in black. For each plot the horizontal axis shows the T_e or n_e just before the puff starts (i.e. ~31 msec before the peak of the gas puff), and the vertical axis shows the values at three successive times, each separated by 33 msec. The T_e points at the peak of the GPI puff in blue circles in Fig. 6(a) are very near to the unity line shown in black, with a linear fit as shown with a slope of 0.93, while at 33 msec and 67 msec after the peak of the GPI puff the linear fits have slopes of 0.81 and 0.74, respectively. The shots with the largest effects in T_e at late times are indicated by the arrow to the green triangles in Fig. 6(a). The decreases in T_e at later times are mainly in the region where $T_e \geq 0.2$ keV, with little or no systematic change in T_e for the edge where $T_e \leq 0.1$ keV, as shown in the log plot in Fig. 6(b). Thus these temperature decreases are localized radially inside the peak of the ionization region of the gas puff. There is also a small systematic increase in density at 33 and 67 msec after the peak of the puff at $n_e \geq 3x10^{13}$ cm^{-3}, some of which is due to the general ~10% per 100 msec increase in average density vs. time in NSTX (see Fig. 2(a)). In the edge region where $n_e \leq 3x10^{13}$ cm^{-3} there is little or no systematic density change at 33 msec and 66 msec after the peak of the puff, as shown in the log plot at the in Fig. 6(d).

The slopes of the linear fits in Fig. 6 are shown in the first entries in Table 3. In addition, the average ratio of electron temperature or density during the puff to that just before the puff is shown by the second entry in this table. For example, the fit to the T_e data at the peak of the gas puff in Fig. 6(a) has a slope of 0.93, and the average ratio of T_e at the peak of the puff to before the puff was 1.10 for these points. The difference between these two numbers is due to different weighting of the points at low and high temperature in these two different statistical measures. Thus there is on average ≤10% change in T_e by the time of the peak of the gas puff in this data.

Figure 7 shows data for the 3rd, 4th, and 5th groups of shots of Table 1 (those without any no-puff comparison shots), plotted in the same way as for Fig. 6. These data are sorted in terms of H-mode shots in Figs. 7(a) and 7(d), L-mode shots in Figs. 7(b) and 7(e), and Ohmic shots in Figs. 7(c) and 7(f), and plotted for three times during the puff. The L-mode and Ohmic shots are generally shorter and less stationary in time than the H-mode shots. The most significant trend is a lower T_e after the puff in the L-mode and Ohmic cases, but there is a relatively large scatter around all the linear fits, partly due to small uncontrolled motion of the separatrix and partly due to turbulent fluctuations in the edge n_e and T_e, as noted previously [3]. Another cause of these variations in H-mode cases is the sharp edge pedestal gradients, which can create relatively large local changes at a fixed radius even for ≤ 1 cm shifts in the location of the separatrix.

Each group of points in Fig. 7 is fit by a linear curve, and the slopes of these fits are summarized in the first entries in Table 3, along with similar fits to the shots from Fig. 6. For the H-mode cases, which are nearest to steady-state conditions without any puff, these slopes are all within 10% of unity for both density and electron temperature at the time of the peak of the GPI puff. All of the other cases have fitted slopes within ±20% of 1.0 at the peak of the puff, and almost all are within 25% of 1.0 at later times.

The same data was also analyzed by finding the average ratio of electron temperature or density during the puff to that just before the puff, as shown by the second entry in each box in this data table. All of these after/before ratios are within 20% of unity at the peak of the gas puff. The Ohmic cases show the largest reduction of the edge electron temperature late in the puff.

2.3 GPI profile data

The only direct measurement of the local effects of the GPI gas puff in this experiment is the radial profile of the GPI Dα emission itself, since this profile depends on the local plasma density and temperature profiles [4]. In this section we describe these profiles for nearly stationary H-mode shots like those in Fig. 2(a).

Figure 8(a) shows a typical image from the GPI diagnostic region of Fig. 1(a). The radial direction is neary horizontal and the vertical direction is nearly poloidal (i.e. perpendicular to the local radial and toroidal directions), with the outward radial direction to the right, and the ion diamagnetic and ion grad-B drift directions downward. The Dα light emission is the vertical orange band just inside (i.e. left of) the magnetic separatrix shown by the dashed line (calculated from EFIT). The projection of the RF antenna limiter is shown by the dotted line, and the GPI gas manifold is shown by the vertical solid line just outside the RF antenna.

The radial profile of GPI emission vs. time was evaluated by averaging over the poloidal range ±10 pixels around the vertical center of these images, i.e. between the horizontal orange lines in Fig. 8(a). In Fig. 8(b) is the time dependence of the radial profile of the GPI light within this vertical band evaluated over the time of the puff, along with the separatrix location (black dashed line). This contour plot was averaged over ~1 msec in time to smooth out the turbulence. The peak of the GPI radial emission profile moves only about 1 cm radially during the duration of the puff (note that the poloidal profile does not vary significantly during the puff).

Figure 9 shows more about the time dependence of the radial profile of the GPI Dα light emission for the same shot as for Fig. 8. Figure 9(a) shows the time dependence of the GPI Dα light emission averaged over the whole GPI field of view, as in Fig. 2. Figure 9(b) shows the time variation of GPI radial profiles with respect to the time-averaged separatrix position, averaged over the vertical band of Fig. 8(a) and over 2.5 msec, with the relative time from earliest (black) to latest (red), following the color scale of Fig. 8(b). The radial peak of the GPI emission remains within 0.5±0.5 cm inside the separatrix over this 80 msec period. Figure 9(c) shows the peak GPI location with respect to the time-averaged separatrix position (black), and the full-width at half maximum of these GPI profiles (blue). The separatrix position vs. time is shown by the red diamond symbols, and varies by ≤ 1 cm during the puff. The main result of Fig. 9 is that the peak location and width of the GPI Dα profiles do not vary by more than ~1 cm during the GPI puff in this case, even though the local neutral deuterium density varies by more than a factor of 10. A similar invariance of the GPI profile during the puff was

noted previously in a different set of NSTX discharges [4]. Note that the GPI profile width does decrease from before the puff to after the start of the puff at 0.593 sec, which is not surprising since without the puff the Dα emission is not toroidally localized.

Figure 10 shows the GPI signal levels, peak locations and widths for a set of six H-mode shots, two from each of the first three shot groups of Table 1. The GPI signal levels in Fig. 10(a) are averaged over the vertical band shown in Fig. 8(a), and the peak locations in Fig. 10(b) and widths in Fig. 10(c) are plotted only after the GPI signal is significantly above the Dα background light. There is no systematic variation in the GPI peak location or width when the GPI signal level rises by at least a factor of ~x5-6, or as the GPI signal level fall by a factor of ~3 over 50 msec after the peak. Thus there is no clear evidence for a systematic variation in the local plasma parameters due to the puff itself; for example, due to a local increase in density, which would tend to shift the emission peak radially outward (see Sec. 3.1). For the Ohmic and L-mode shots of Table 1 there is sometimes up to a ~2 cm shift of the peak GPI location vs. time during the puff, mainly correlated with shifts in the separatrix position during these relatively non-stationary discharges, and not systematically correlated with the puff itself.

2.4 GPI turbulence analysis

Figure 11(a) shows an example of the time dependence of the GPI signal within the small 1.5 cm square region shown in Fig. 8(a), which is centered at a radius 1 cm inside the separatrix position for this shot. The time average of the signal in this region (orange line) is very similar to the average over the whole frame for a similar shot in Fig. 9(a). Figure 11(b) shows the frequency spectrum of the normalized amplitude fluctuations in the GPI signal in this square region vs. time, i.e. of the signal divided by its value smoothed over 1 msec, with the spectral amplitude scale shown by the color bar at the upper right. In this example the normalized fluctuation spectrum is very similar from the very beginning of the puff (0.595 sec) through 55 msec after the peak of the puff (0.670 sec). For other radii and other shots the spectra are not always so constant vs. time, but there is no general systematic variation of the spectrum shape vs. time during these gas puffs.

Figure 12 shows the analysis of several turbulence quantities for the same six H-mode shots used for Fig. 10. Figure 12(a) shows the GPI signal levels within the small square regions 1 cm inside the separatrix, which are all similar. Figures 12(b) and 12(c) are the relative GPI fluctuation levels (rms/mean) and autocorrelation times (FWHM), which show no systematic variation during these puffs. Figure 12(d) and 12(e) are the correlation lengths between this region and similar square regions located 1.5 cm below (for L_{pol}) and 1.5 cm farther inward (for L_{rad}), calculated as in [42]. There is no systematic variation in these correlation lengths over the time of these puffs. Finally, Fig. 12(f) shows the poloidal velocity V_{pol} calculated as in [42] using data from individual pixels and time delays of up to 10 μsec. Again, there was no systematic variation in these turbulence velocities over the time of these puffs. The radial velocities (not shown) were

much smaller than the poloidal velocities for these H-mode cases, and were all within ±1 km/sec of zero.

The conclusion from this analysis is that the local edge turbulence as measured by the GPI diagnostic itself does not vary as the influx rate of the gas puff varies by at least a factor of x5, at least for H-mode discharges. This implies that the GPI gas puff itself does not significantly perturb the edge turbulence in these typical cases. It is interesting to note that the edge turbulence is not substantially different among the six shots shown in Fig. 12, which have a range of NBI power from 2-6 MW and different global parameters (see Table 1). This shows that the edge turbulence in NSTX is relatively insensitive to the edge plasma parameters, at least for these H-mode plasmas.

2.5 Other diagnostic data

Figure 13 shows several other signals as a function of time during the GPI puff for the same shots as in Fig. 2(a), in which one shot has no gas puff (#138843) and the three successive shots have a GPI gas puff (top panel). Recall that these are the shots which showed the largest effect of the gas puff on the edge plasma temperature among the first two groups of shots (see Fig. 6). Figure 13(a) shows the GPI gas puffs, and Fig. 13(b) shows an ultra-soft x-ray signal chord with a tangency radius 3.5 cm inside the separatrix [43], which has only a slight increase at the time of the puff. Figure 13(c) shows the outer separatrix locations, which have no significant variation during the puff. Figure 13(d) shows Dα signals from the lower divertor region, which do have a significant increase with the GPI puff, most likely due to parallel transport of ions from the GPI puff region to the divertor plate. Figure 13(e) shows the total radiated power in the main plasma volume, which has little or no change with the puff. Finally, in Fig. 13(f) are the neutron signals, which decrease by ~10-20% over ~50 msec after the peak of the puff, perhaps reflecting the decrease in electron temperature shown in Fig. 4. In general, these other diagnostic signals (except for the divertor Dα) show only a small effect of the GPI puff on the edge and core plasma.

Figure 14 shows the edge ion temperature and rotation speed measured for all of the shots in Table 1 using the NSTX edge rotation diagnostic, which is based on passive visible spectroscopy of CIII [44]. The ion temperature in Fig. 14(a) and toroidal velocities in Fig. 14(b) were evaluated at the peak of the radial emission profile of this line, which is typically located a few centimeters inside the separatrix. Linear fits to these data are shown by the lines, which show little or no systematic change in T_i or V_{tor} after the puff. A similar plot of V_{pol} shows no significant variation with the puff, but with V_{pol} within ±20 km/sec of zero. The active CHERS data was not available due to interference of the GPI puff with the background CHERS signal.

Figure 15 shows data from the beam emission spectroscopy (BES) diagnostic, which measures the Dα light emission from the NBI. Figure 15(a) shows an increase in

BES signal level which follows the Dα emission during the GPI puff in shown in Fig. 15(d), to within the uncertainty in the mutual timing. This particular BES signal from ~3 cm inside the separatrix increases because this sightline is within ~40 cm of the GPI gas puff, and the BES is affected by the neutral deuterium density in its vicinity. The fluctuation level seen by the BES above 4 kHz in Fig. 15(b) also increases with the GPI puff, such that the RMS level of the fluctuations above 4 kHz normalized to the low pass filtered signal in Fig. 15(c) is not significantly affected by the GPI puff. A detailed comparison of BES and GPI fluctuations will be presented elsewhere [45]. Signals from the high-k scattering diagnostic viewing nearest the edge at R~138±2 cm also show no qualitative change with the GPI puff, e.g. at $k_\perp \rho_s = 16$. There is also no visible effect of the GPI gas puff on the MHD activity as measured by the magnetic fluctuation coils inside the vacuum vessel.

2.6 L-H transition and ELMs

None of the 27 shots in Table 1 had an L-H transition or an H-L transition during the time of the GPI gas puff, which shows that this puff does not necessarily trigger either a transition or a back-transition in NSTX. There were 23 other shots in the 2010 run which did have an L-H transition during the GPI puff duration period, mainly because the GPI puff was purposely triggered to catch these transitions. In those cases the time of the L-H transitions varied between ~18-105 msec after start of the puff, i.e. without any clear correlation to the influx rate from the GPI puff. Earlier studies of the L-H transition in NSTX also showed no effect of the GPI puffing on the L-H transition [46].

Similarly, there is no evidence that the GPI gas puff affects ELMs in NSTX. The shots in Table 1 were chosen to avoid ELMs during the GPI puff, therefore the puff does not necessarily trigger ELMs. However, there were many other shots with ELMs during the GPI puff (e.g. in [4]), and previous studies were made of the 2-D structure and motion of ELMs using GPI data [47,48], so the puff does not suppress ELMs either. It is not clear why injection of small deuterium pellets can suppress ELMs [37] while a gas puff with a similar time-averaged neutral influx does not.

3.0 Modeling

At present there is no complete model for the effects of a deuterium gas puff on these NSTX plasmas. Sections 3.1 and 3.2 apply the existing codes DEGAS 2 and UDEGE to partially model one shot in this run. Section 3.3 then describes simplified generic estimates for the local and edge effects of this gas puff, including a discussion of their limitations.

3.1 DEGAS 2 modeling

Three-dimensional DEGAS 2 simulations for four times during shot 138846 have been run in the manner described in Ref. [4]. These simulations use an EFIT equilibrium to define the flux surface shapes in the vicinity of the GPI viewing area. The electron density and temperature values obtained from the Thomson scattering diagnostic are mapped onto these, assuming that they are constant on flux surfaces. One improvement relative to the procedure in Ref. [4] is that data from the CHERS diagnostic are used to estimate a fixed ratio of the deuterium ion to electron density ratio. Since we have no *a priori* reason to believe that T_i differs significantly from T_e and since the CHERS data do not extend into the GPI emission region, we assume $T_i = T_e$.

Deuterium molecules are sampled randomly from a 300 K thermal energy and cosine angular distribution across ten 2 x 2 cm squares that represent the GPI gas manifold; the squares are aligned with the pitch of the actual manifold. As the molecules penetrate the plasma, they undergo ionization, dissociation, and elastic scattering; resulting molecular ions are assumed to be ionized, dissociated, or recombined immediately. Any product atoms are then tracked through the plasma and interact with it via ionization and charge exchange. The principal output of the DEGAS 2 calculations is the simulated view of the GPI camera obtained by integrating the $D\alpha$ emission from atoms and molecules along chords corresponding to each of the camera's 80 x 64 pixels. The reader is referred to Ref. [4] for additional details.

To estimate the dimensions and volume of the emission region, we construct 2-D slices through the simulation volume both parallel and perpendicular to the gas manifold, with the latter being roughly indicative of the variation parallel to the magnetic field. From each, we obtain the full width at half-maximum of the emission profile. The widths parallel to the manifold and the magnetic field are comparable, L_o~15 cm. The radial width is much more narrow, 2–3 cm, reflecting the steepness of the plasma profiles. This width is somewhat less than the measured width of ~4-5 cm for this shot in Fig. 10(c), probably due to the broadening effects of the finite toroidal width of the gas cloud and plasma turbulence in the actual shot. The overall shape of the emission region is that of a disk, i.e., a flat cylinder. The corresponding estimate of its volume is 350 – 540 cm^3.

The volumetric sources of plasma particles and energy computed in these simulations can be integrated over flux surfaces for the purpose of estimating the global impact of the gas puff on the plasma. Figure 16(a) shows radial profiles of these energy source rates for the simulation of 138846 at the time of the peak puff rate, 0.615 s, and scaled to a peak neutral gas source rate of 6.6×10^{21} atoms/s; the volumetric photon emission rate is included in the figure for reference. These source rates can in turn be summed over the volumes inside and outside the separatrix, as well as over the entire volume, as shown in Table 4. The calculated ionization rate inside the separatrix is 1.8×10^{21} atoms/sec, which is 27% of the neutral gas puff rate. This is somewhat higher than estimates of 'fueling efficiency' of 0.05-0.20 deduced for other gas puffing systems in NSTX [49].

Note that these DEGAS 2 runs have been designed to simulate the plasma-neutral interactions only in the vicinity of the GPI camera view and that a significant fraction

(~1/3) of the neutral atoms and molecules leave the simulation volume without being ionized. Note also that the dividing line between source rates inside and outside the separatrix in Fig. 16 and Table 4 depends on the accuracy of the EFIT02 equilibrium reconstruction of the separatrix location, which could be uncertain by up to about ±2 cm.

The electron energy losses are roughly evenly split between those due to atoms (ionization, line radiation) and molecules (dissociation and ionization). Overall, the ions lose 18 kW, effectively heating deuterium atoms via charge exchange, but gain 13 kW of this back when those atoms are ionized, because the warm atoms then become ions (again). Therefore the direct energy loss rate due to atomic physics processes in the gas cloud is negligible compared with the power flow from the main plasma through the edge flux surfaces, which is ~4 MW for this shot.

DEGAS 2 simulations of shot 138846 were done at four times relative to the peak time of the puff (0.615 s): -20, 0, +30, +70 ms, based on the Thomson scattering measurements of n_e and T_e made at the other side of NSTX. Radial profiles from both the simulated and experimental camera images are obtained by integrating over 20 pixels around the vertical center of the frame (red lines in Fig. 8). The radial locations of the peaks of these profiles, mapped to midplane and relative to the separatrix, are shown in Fig. 16(b). The error bars reflect an uncertainty of ±1 pixel (0.3 cm), based on Refs. [4] and [50]. Note however that the radial separation between Thomson edge channels is 2 cm, so any resolution finer than this is based on interpolation.

The simulated DEGAS 2 radial profile peak locations for three of the four radial points are within the error bars of the observed GPI peak locations, as was also found previously for four other H-mode shots [4]. The largest deviation in the DEGAS 2 peak location in Fig. 16(b) is at +30 msec (0.645 sec), where it was ~2 cm farther radially outward than the observed GPI peak in this shot, possibly indicating a difference between the n_e and T_e in the GPI gas cloud and the Thomson scattering measurements on the same flux surfaces. Note however, that the radial excursion of the simulated peak location tracks the separatrix temperature (dashed line in Fig. 16(b)), allowing us to use the Thomson scattering profile as a proxy for DEGAS 2 simulations of other shots. An examination of the Thomson scattering profiles of shots 138844 and 138845 does not show a pattern similar to that of 138846 (Fig. 5), leading to the conclusion the discrepancy seen at 0.645 sec is most likely due to a random turbulent fluctuation seen by the Thomson scattering for this point in space and time, which is not accounted for in the depicted error bars [50].

A rough evaluation can be made of the expected radial shift of the emission peak in response to a local change in the density. The variation of the Dα emission rate with n_e and T_e for plasma parameters typical of the emission peak (e.g. T_e ~ 30-70 eV) is expected to be $n_e^{0.4}$ if the temperature change is inversely proportional to the density change. Using this scaling and the plasma gradients near the peak, we find that a doubling of the density would shift the emission peak by ~0.5 cm. This is marginally within the resolution of these measurements, so that the Dα profile measurement can only

discern a local density change larger than a factor of two. Estimates of the gas puff effects on the local plasma parameters are further discussed in Sec. 3.3.

3.2 UEDGE modeling

UEDGE, a two-dimensional (axisymmetric) multi-fluid edge transport code [51], was used to evaluate the effects of the GPI gas puff on the NSTX edge plasma for shot 138846 (same shot as for Sec. 3.1). A narrow slice of the edge and SOL is captured; at the outer midplane, the grid extends from 1.92 cm inside the separatrix to 0.65 cm into the SOL. The separatrix location is calculated self-consistently with the expected SOL heat flux and is ~1 cm farther in than the EFIT02 separatrix used in DEGAS 2. Parallel transport is treated with the flux-limited Braginskii equations [52], perpendicular transport is modeled with assumed anomalous perpendicular diffusivities (with no pinch) to fit the pre-puff plasma profiles, and a fluid neutral model employed. Carbon radiation is included, assuming a fixed 5% carbon concentration, consistent with midplane C^{6+} density measurements. Radially-varying diffusivities are adjusted such that UEDGE midplane temperature and density profiles approximately match midplane Thomson data. This simulation also includes the particle source from the center stack gas puff and NBI, which were the same for shots with and without the GPI gas puff, and an assumed divertor recycling coefficient of 0.9.

After establishing a steady-state solution, an axisymmetric model of the GPI gas puff is introduced, and the time-dependent edge plasma behavior is tracked. This gas puff rate rises linearly for 20 msec to 2.6×10^{21} s^{-1}, which is the peak deuterium gas flux into the UEDGE domain based on DEGAS 2 results (Sec. 3.1). After the peak, the puff decays exponentially with a 50-msec decay time. The UEDGE modeling shows a relatively strong edge plasma response, as seen by the outer midplane ion and neutral densities, and ion and electron temperatures in Fig. 17. The calculated ion density at the separatrix increases by ~50% by the time of the peak of the puff, and by 30 msec after the peak of the puff the calculated ion density at the separatrix rises by about a factor-of-two from 0.8×10^{13} to 1.5×10^{13} cm^{-3}, i.e., $\delta n = 0.7 \times 10^{13}$ cm^{-3}. The latter is not far from the observed increase in density seen for this particular shot at the separatrix at 35 msec after the peak of the puff in Fig. 5(c), although the density rise due to these puffs is typically less than 25% at this time (see Table 3). The neutral density due to the gas puff at the separatrix rises to ~5×10^{10} cm^{-3}, but the local neutral influx due to the gas puff is ≤25% of the calculated neutral influx due to recycling at the divertor.

This calculated rise in edge density can be interpreted in terms of an edge particle confinement time $\tau_{p,UEDGE} = (\delta n \, V_{UEDGE}) / \Gamma_{o,in}$, where $V_{UEDGE} = 2.5 \times 10^{6}$ cm^{-3} is the simulation volume and $\Gamma_{o,in} = 1.3 \times 10^{21}$ s^{-1} is an average rate of GPI puff ionization inside the separatrix for the modeled time period. This results in a $\tau_{p,UEDGE}$ ~10 ms, which is significantly higher than the estimated edge energy confinement time (see Sec. 3.3). This relatively large edge density rise is partially due to the large recycling at the divertor plate and to the divertor detachment, which occurs in this simulation due to the GPI puff.

Some features of the UEDGE solution disagree with experimental data: the simulated density and temperature changes are larger than observed changes, and outer divertor detachment is not seen experimentally. Thus this simulation should be considered as a first attempt at modeling this gas puff, and additional physical effects missing from this preliminary simulation might be unveiled by future model refinement.

3.3 Simple estimates for the edge effects of the gas puff

We first estimate the maximum local density perturbation expected due to this gas puff for shot #138846, which was modeled in Sections 3.1 and 3.2. Newly created ions are assumed to be lost from the neutral gas cloud only by parallel motion along B with a typical deuterium ion sound speed of c_s~$5x10^6$ cm/sec assuming T_e~50 eV near the peak of the ionization rate (i.e. $c_s/2$ in both directions). If there is no return of these ions to this birth region, the local density rise within the ionization volume V_o for a neutral influx rate of Γ_o should be $\delta n_{local} \sim (\Gamma_o/V_o)(L_o/c_s)$, where L_o is its cloud length along B, with typically L_o~15 cm and V_o ~ 450 cm^3 from DEGAS 2 modeling (Sec. 3.1). The ion loss time from this volume is (L_o/c_s) ~ 3 μs, i.e. less than the turbulence timescale, so the turbulent motion should not affect this loss rate. Given a peak ionization rate of Γ_o~$4.4x10^{21}$ atoms/sec over the whole gas cloud (Table 4), the average density perturbation within the GPI gas cloud at this time should then be δn_{local}~$3x10^{13}$ cm^{-3}, and the radial profile of this perturbation should be the similar to the photon emission profile shown in Fig. 16(a). This estimated density rise is comparable to the density measured by Thomson scattering near the peak location of the ionization ~1.4 cm inside the separatrix in Fig. 4(c), but much larger than the density measured in the SOL in Fig. 5(c)-(d). However, since the Thomson scattering was located on the other side of the machine and far from the magnetic field lines going through the GPI gas puff, this local density increase is not expected to be measured there.

On a longer timescale, the ions born inside the separatrix will travel along B and fill up the volume of the flux surfaces on which they were born, which extends roughly δr_{in} = 3 cm radially inside the separatrix at the outer midplane (Fig. 5(b)) over a volume of $V_{edge} \sim (4\pi^2 Ra)\, \delta r_{in}$~0.6 m^3. The density increase on these flux surfaces will depend on the edge ion particle confinement time, which is not directly measured. If we assume that the edge particle confinement time is related to the edge energy confinement time by $\tau_{p,edge} \sim \tau_{E,edge}/(1-R)$, where $\tau_{E,edge}$~0.2 msec (see Sec. 3.3.2) and R=0.9 is the assumed recycling coefficient (Sec. 3.2), then $\tau_{p,edge}$~2 msec, and the estimated rise in edge density averaged over the flux surfaces of the gas cloud due to an ionization source of Γ_{in} $=1.8x10^{21}$ D/sec (Table 4) is $\delta n_{in} = \Gamma_{in}\, \tau_{p,edge} / V_{edge} \sim 6x10^{12}$ cm^{-3}. This is roughly consistent with the UEDGE modeling, but the actual recycling and edge particle confinement time are not known well enough for a more quantitative comparison with the experimental results.

Next we estimate the maximum edge temperature perturbation expected inside the separatrix due to the energy loss rate of P_{puff}~10 kW from radiation and CX from the gas

puff (Table 4). The perpendicular cross-field heat flux through the gas cloud region for shot #138846 can be roughly estimated by assuming the input power is lost over an area ~$(2\pi R)(\pi a)$ near the outboard midplane, i.e. $P_{edge}/2\pi^2 Ra \sim 4$ MW/2x10^5 cm$^2 \sim 20$ W/cm^2. Over the cloud area ~15 cm x 15 cm ~ 200 cm^2 within a flux surface, this perpendicular heat flow is ~5 kW, which is comparable to the radiated power from the gas puff cloud. However, the heat flux coming from upstream along the B should be much larger than the local perpendicular heat flux energy across the gas cloud. Therefore the local radiated power from the gas cloud can create only a small local change in the edge temperature, so it seems reasonable to assume that the edge temperature is nearly constant all along a flux surface through the gas cloud.

With this assumption of constant electron temperature along a flux surface and $T_i=T_e$, we can estimate the edge energy confinement time and then evaluate the effect of the gas puff radiation on the edge temperature. Within the region between ρ=0-3 cm inside the separatrix, the plasma just before the gas puff has an average T_e=150 eV and n_e =2x10^{13} cm^{-3}, so the total stored energy in this volume is W_{edge}~1 kJ. The edge energy confinement time is $\tau_{E,edge} \sim W_{edge}/P_{edge}$, where P_{edge} is the power flowing from the main plasma into the edge region. For a shot like #138846, $P_{edge} \sim 4$ MW, thus $\tau_{edge} \sim 1$ kJ/4 MW ~ 0.2 msec. Assuming this τ_{edge} does not change significantly vs. time with the GPI puff, the edge stored energy near the peak of the puff should therefore be $W_{puff} \sim (P_{edge} - P_{puff})/\tau_{E,edge,}$ which is very nearly the same as W_{edge} since $P_{puff} \leq 10^{-2} P_{edge}$. Thus the edge temperature within this region should not decrease due to the puff radiation, but should only decrease by the same fractional amount as the edge density increased during the puff. This is approximately consistent with most of the data in Figs. 6 and 7 and the statistical fits of Table 3, in which these changes are almost all ≤20%.

It is not yet clear how well these simple estimates compare with the actual local density and/or temperature changes within the GPI gas cloud region, since these were not directly measured in this experiment. There are other mechanisms of heat flow into and out of this magnetic flux tube which should be taken into account, such as poloidal or toroidal plasma flow or neoclassical particle drifts. Therefore a 2-D or 3-D model of the heat balance of the gas cloud will probably be needed to calculate the local cooling effect of the cloud radiation. This model should also include the background impurity radiation, which is very likely larger than the radiation from the deuterium in the gas cloud when averaged over an edge flux surface.

4.0 Discussion

Section 4.1 compares the experimental results and modeling in this paper with previous work, Section 4.2 discusses unresolved issues and future directions, and in Sec. 4.3 are the conclusions.

4.1 Relationships to previous experiments and modeling

As mentioned in the Introduction, previous deuterium gas puffing experiments on the PBX-M [5], ADITYA [8,9] and STOR-M [10] produced significant perturbations in the edge plasma and the edge turbulence. However, gas puffing done for the GPI measurements on Alcator C-Mod [11,12], EAST [13], and TEXTOR [14] reported no significant perturbations of the gas puff on the edge turbulence, and the present paper basically confirms those results. In general, it is not yet clear what parameter(s) determine the threshold at which a gas puff begins to cause a significant perturbation. This threshold should depend on the gas puff rate, but also on the plasma size, heating power, magnetic geometry, edge particle confinement, edge impurities and radiation, divertor recycling rate, the gas puff location and spatial distribution, and probably other parameters as well. Thus we cannot yet establish a comparative quantitative relationship between the gas puff effects in the present and those in previous experiments.

Most previous modeling of deuterium gas puffing was done to help understand and control divertor plasma detachment. This modeling usually assumed constant gas puffing with simplified edge transport models in codes like UEDGE [35] and SOLPS [53]. The UEDGE modeling of the pulsed gas puff in Sec. 3.2 predicted increases in the density at the separatrix which were larger than those observed, and the formation of a detached plasma, which was not observed. Thus this model needs to be further refined and validated for gas puff experiments of this type.

Prior experiments and modeling of deuterium gas puffing was also done in the context of ideas to understand or control the L-H transition [25,29]. Experimental results previously showed that the L-H transition in NSTX and MAST depended on the location of the gas fueling source [18,19], which was modeled by the neutral effects on poloidal rotation [27]. However, as described in Sec. 2.6, the gas puffs in the present experiment had no effect on the L-H transition, either to trigger an H-mode from an L-mode plasma or *vice versa*. This is consistent with the absence of any visible effects of this puff on the edge turbulence or edge plasma velocity in these experiments.

The effects of lithium wall coating on the edge transport and stability have been previously modeled for NSTX using both SOLPS [54] and the microinstability code GS2 [55]. Increased lithium coating can apparently reduce the recycling coefficient and change the edge pressure gradients, which may then affect the edge turbulence and edge transport. The discharges described in this paper had a wide range of lithium coatings (see Table 1), apparently with no systematic influence on the deuterium puffing results.

Measurements and modeling of the local effect of a strong gas puff on plasma near the density limit were done in TEXTOR in the radiation increased confinement (RI) regime [16]. At deuterium gas fueling rates up to 9×10^{20} D atom/sec over ~3 sec, the local density near the gas puff location increased by up to a factor of ~4 and the local temperature decreased from ~50 eV to ~10 eV. These changes were fit with a 2-point model, but it is not clear how these TEXTOR results with neon seeding near the density limit are related with the present experiments, which were not near the density limit and

had no impurity seeding. The latest versions of this model were applied to impurity puffs during massive gas injection [33], and could also be applied to the present experiment.

4.2 Unresolved issues and future directions

The largest unresolved experimental issue in this paper is the effect of the gas puff on the local density and temperature within the gas cloud. The only measurements within the gas cloud were the $D\alpha$ profiles from the GPI diagnostic, which showed no systematic change with time during the gas puff. It might be possible in the future to infer the local temperatures and densities within the cloud using helium gas mixed into the puff with 2-D imaging the HeI line ratios [55,57]. Local measurements might also made using a Langmuir probe, and it would be interesting to compare the perturbation due to the probe with that due to the gas puff.

The most surprising experimental result was an occasional decrease in edge electron temperature well after the peak of the puff and inside the radius of its peak ionization, as illustrated in Figs. 3-5. This decrease occurred on the timescale of ~50-100 msec, and not before the time of peak gas influx rate. This suggests that it may be related to the surface state of the wall or divertor plates, i.e. a higher recycling rate might cause the injected gas to be better retained in the edge. In general, the relationship between wall and divertor recycling and tokamak confinement is still an important and largely unresolved issue.

The deuterium gas puffs used in these experiments did not affect the L-H transition. Further experiments with a higher gas puff influx rate or longer puff duration would help to connect these results to previous measurements which showed such an effect [18,19]. Future modeling will need to explain the L-H transition in existing discharges and predict its dependence on edge plasma parameters, in order to determine the threshold at which a gas puff will begin to influence the transition in a particular discharge. This modeling should also take into account the X-point geometry and recycling, since these can affect the L-H transition in NSTX even without any explicit consideration of edge turbulence [58].

There are clearly unresolved issues concerning the theory and modeling of the local gas puff effects on the edge plasma. A primary issue is how to calculate the local temperature and density perturbations, given that the heat and particle transport mechanisms in at least two of these three dimensions are not well understood. Progress on this general problem has been made recently and comparisons with massive impurity gas puffing have been made [32,33]. A comprehensive model for these processes in NSTX should include 3-D transport effects, the background edge impurity content and radiation, edge plasma rotation, neoclassical transport, flux surface shaping, and divertor radiation and recycling.

One of the motivations for this paper was to evaluate the possible perturbing effect of the GPI gas puff on the edge turbulence, and the result is that there appears to be no significant perturbing effect. This is not too surprising since even large changes in discharge parameters caused little change in the edge turbulence [42], e.g. varying the

NBI power from 2-6 MW in the H-mode shots of Fig. 12. The edge turbulence NSTX has not yet been explained by turbulence simulations, and in particular the expected sensitivity of the turbulence to neutral gas sources is still unknown, although progress in this area is beginning to be made with the edge turbulence simulation code XGC-1, which is capable of treating the effects of neutrals [59]. A complete model for this experiment should include the specific effects of the 3-D localized gas puff on the edge turbulence. A related analysis of the gas puff charge exchange diagnostic has recently been done on Alcator C-Mod [60].

The experimental work on NSTX should also be extended to include the analysis of other diagnostic data such as divertor heat flux IRTV measurements, visible imaging of edge and divertor impurity and Dα emission, edge and core impurity content, neutral density measurements, reflectometer edge density and fluctuation profiles, USXR profiles, and ion temperature and rotation profiles.

4.3 Conclusions

This paper describes in considerable detail the effects of a small pulsed deuterium gas puff on the edge plasma and edge turbulence in NSTX. This gas puff caused little or no change in the line-averaged plasma density or total stored energy, and the edge density and electron temperature changed by ≤10% by time of the peak of the gas puff. However, in some discharges there was a ~20-30% decrease in the edge electron temperature ~50-100 msec after the peak of the puff, the cause of which is not yet understood. The radial profile of the Dα light emission from this gas puff as seen by the gas puff imaging (GPI) diagnostic did not vary significantly over the rise and fall of the gas puff influx rate, which is consistent with nearly constant edge electron temperature and density profiles in the gas cloud ionization region. The edge turbulence seen in the GPI diagnostic (and other edge turbulence diagnostics) did not vary significantly with time during the puff.

Therefore we conclude that the GPI gas puffs used in these NSTX experiments did not significantly perturb either the plasma parameters or the edge turbulence in the region of the Dα emission from these puffs, at least up to the time of the peak of the GPI gas puff influx rate when most of the previous GPI turbulence measurements have been made. The possible effects at later times should be evaluated on a case-by-case basis.

Modeling of the Dα light emission with DEGAS 2 was consistent with observed GPI images, at least to within the uncertainty of the edge density and temperature profiles as measured by Thomson scattering. Initial UEDGE modeling based on steady-state profiles predicted a factor-of-two increase in edge density and decrease in edge temperature by ~30 msec after the peak of the puff, which are larger than observed; therefore further dedicated experiments and modeling are needed to in order understand the reasons for these differences. Future experiments should be done with a larger range of deuterium gas puff influx rate and duration in order to help clarify the scaling of these effects.

Acknowledgments:

The authors would like to thank the NSTX group and particularly D. Battaglia, A. Diallo, and S. Kubota for the gas puffing during their experiments, S. Gerhardt, K. Tritz, S. Sabbagh, H. Schneider, and F. Scotti for help with diagnostic data, C.S. Chang, J. Lang, R. Maingi, and J.L. Terry for discussions on this topic. This work was supported by US DOE Contract # DE-AC02-76CH03073.

Table 1: Shot list

shot	B(kG)	I(MA)	P(MW)	n[(a)]	gap[(b)]	Li[(c)]	peak[(d)]	puff[(e)]	Plasma type
138843	4.4	0.8	3.9	6.5	10.2	104	0.613	0	NBI H-mode
138844	4.4	0.8	3.9	6.5	10.1	112	0.613	5.7	NBI H-mode
138845	4.4	0.8	3.9	7.0	10.0	101	0.613	5.4	NBI H-mode
138846	4.4	0.8	3.9	7.1	10.1	104	0.613	5.7	NBI H-mode
139494	4.7	0.9	2.0	6.7	11.6	152	0.512	5.9	NBI H-mode
139495	4.7	0.9	2.0	6.1	11.5	152	0.512	0	NBI H-mode
139499	4.7	0.9	2.0	6.4	11.2	153	0.512	5.4	NBI H-mode
139500	4.7	0.9	2.0	6.3	11.4	152	0.512	5.5	NBI H-mode
139501	4.7	0.9	2.0	6.6	11.4	152	0.512	5.4	NBI H-mode
139044	4.9	1.0	6.0	5.7	10.3	0	0.412	5.4	NBI H-mode
139048	5.4	1.1	6.0	5.0	11.3	96	0.412	5.8	NBI H-mode
139286	4.9	0.8	3.0	3.7	10.9	293	0.314	5.7	NBI H-mode
139508	4.4	0.8	3.0	5.1	11.4	151	0.412	4.6	NBI H-mode
139509	4.4	0.8	3.0	4.5	11.8	141	0.412	4.3	NBI H-mode
139510	4.4	0.8	2.0	5.1	11.6	140	0.412	4.3	NBI H-mode
139443	5.4	1.1	0	2.9	9.9	81	0.287	4.8	Ohmic
141911	4.4	0.9	0	3.0	6.3	0	0.285	3.5	Ohmic
141912	4.4	0.9	0	3.0	6.5	0	0.285	3.5	Ohmic
141740	4.4	0.8	0	1.7	8.9	0	0.213	5.9	Ohmic
141741	4.0	0.7	0	1.9	9.3	0	0.213	5.7	Ohmic
141742	4.4	0.8	0	1.7	8.3	0	0.213	6.0	Ohmic
141754	3.6	0.8	0	2.0	8.6	0	0.213	5.7	Ohmic
141756	3.6	0.8	0	2.0	8.7	0	0.213	5.9	Ohmic
139441	5.4	1.1	2.0	2.5	10.1	80	0.287	5.4	NBI L-mode
139442	5.4	1.1	2.0	2.7	10.0	80	0.287	5.7	NBI L-mode
141984	4.4	0.9	1.1	2.5	2.8	0	0.224	3.7	RF L-mode
141985	4.4	0.9	1.1	2.5	3.1	0	0.224	3.5	RF L-mode

a) line integrated density $x10^{15}$ cm^{-2}
b) distance between separatrix and outer midplane RF antenna structure at 157.5 cm
c) amount of lithium wall coating just before shot (mg)
d) time of the peak of the GPI puff (sec)
e) total GPI gas puff in Torr-liters

Table 2 – deuterium gas puff parameters (#138846)

	by the time of peak of puff (0.613 sec)	by 67 msec after the peak (0.680 sec)	All gas puff duration (0.593- 0.800 sec)
neutrals puffed	7.6×10^{19} D atoms	3.0×10^{20} D atoms	3.8×10^{20} D atoms
neutral influx rate	6.6×10^{21} D atoms/sec	3.2×10^{21} D atoms/sec	1.8×10^{21} D atoms/sec
total plasma electron content	~6×10^{20} electrons	~6.4×10^{20} electrons	---

Table 3 – Thomson data for linear fits and after/before ratios vs. time during GPI puff

	GPI peak (fit/ratio)	+ 33 ms (fit/ratio)	+ 67 ms (fit/ratio)
T_e (H-mode Fig. 6)	0.93/1.10	0.80/0.99	0.74/0.94
T_e (H-mode Fig. 7)	1.00/1.00	0.95/0.93	0.98/0.88
T_e (L-mode Fig. 7)	1.19/1.09	1.20/1.05	0.95/0.96
T_e (Ohmic Fig. 7)	0.92/0.81	0.90/0.66	0.81/0.61
n_e (H-mode Fig. 6)	1.00/1.23	1.04/1.34	1.07/1.29
n_e (H-mode Fig. 7)	1.07/1.06	1.11/1.13	1.33/1.06
n_e (L-mode Fig. 7)	1.08/1.15	1.25/1.16	0.88/1.30
n_e (Ohmic Fig. 7)	1.00/1.15	1.20/1.07	1.26/1.03

Table 4 - DEGAS 2 138846 @ 0.615 s volume integrated source and loss rates.

	Peak ion source rate (D^+/s)	Peak ion power loss (kW)	Peak electron power loss (kW)
Inside separatrix	1.8×10^{21}	4.0	6.5
Outside separatrix	2.6×10^{21}	0.05	14.5
Total	4.4×10^{21}	4.0	21

Figure Captions

1. A cross section of NSTX for a typical shot in (a), and a picture of the GPI hardware inside the vessel is shown in (b). The GPI gas puff manifold is attached to the outer wall ~20 cm above the midplane and about 2 cm behind the shadow of the nearby RF antenna limiter. The GPI Dα light emission is viewed over the region shown in (a) using the optical viewport shown in (b).

2. Part (a) shows the time dependence of the plasma current, neutral beam injected (NBI) power, line averaged electron density, and the average GPI Dα light emission within the field of view of Fig. 1 for the first group of shots of Table 1. Shot 138843 had no GPI puff, while the three successive shots have similar GPI puffs. There is no visible effect of the GPI puff on the time evolution of the line-integrated electron density in these cases. Part (b) shows the total stored energy before vs. after the GPI puff for all the shots of Table 1, again showing no systematic effect of the puff. Points in black are with no GPI puff.

3. Comparison of the Thomson scattering profiles for shots without a GPI gas puff (a) and with a GPI gas puff (b) as a function of time, along with the line-integrated density, central electron temperature, and GPI Dα signals below each. The separatrix is shown by the dashed white line, and the contour lines correspond to the marks on the colorbar at the right. The density profile does not appear to be significantly affected by the gas puff, but there appears to be some change in the edge temperature after the peak of the puff.

4. Time dependence of T_e and n_e measured by Thomson scattering over ±0.3 sec around the GPI puff time for the shots in Fig. 2(a), one without (138843) and three with a puff. The total Dα light vs. time from the GPI puff is shown by the black dots at the bottom of each plot. The edge T_e decreases ~50 msec after the puff starts for regions more than ~3 cm inside the separatrix, and the n_e increases slightly over ~50 msec after the puff starts for regions within ~5 cm of the separatrix.

5. Radial dependence of T_e and n_e measured by Thomson scattering for the same four shots as Fig. 4, including one shot with no GPI puff (138843). The horizontal axis is the distance from the outer midplane separatrix for each shot. Part (c) and (d) show that T_e decreases significantly 36 msec and 70 msec after the peak of the GPI puff, but only at radii more than ~3 cm inside the separatrix. The shot-to-shot the differences in the radial location of the data points are due to the slightly different separatrix locations, as listed in Table 1. The radial profiles of the gas puff Dα emission are shown by the black dots in the T_e plots.

6. Comparison of T_e and n_e between the time just before the GPI puff (horizontal axis) and three times after the GPI puff (vertical axis) for all points in the first two groups of shots in Table 1. Shots with no gas puff are shown in black symbols. The same data is shown in a linear scale in (a) and (c) and a log scale in (b) and (d). There is a significant decrease in T_e at 33 msec and 66 msec after the peak of the puff for points at $T_e \geq 0.3$

keV, but not for $T_e \leq 0.3$ keV. In many (but not all) cases there is a significant increase in the edge region where $n_e \leq 3x10^{13}$ cm^{-3} at 33 msec and 66 msec after the peak of the puff.

7. Additional Thomson scattering data in the same format as Fig. 6, but for the 3rd, 4th, and 5th groups of shots of Table 1 (which do not have comparison shots without a GPI gas puff). On the horizontal axes are the T_e and n_e just before the GPI puff, and on the vertical axes are the T_e and n_e at three times during the GPI puff. This data is sorted in terms of H-mode shots (a), L-mode shots (b), and Ohmic shots (c). Linear fit are made to the data for each time and the slopes of these fits are shown in Table 3. There is generally $\leq 25\%$ systematic variation in the edge T_e and n_e due to the puff, although there is considerable random scatter in the data.

8. Part (a) shows a typical image of the ~25 cm x 30 cm region of the GPI gas puff just above the outer midplane of NSTX, with the radial direction is approximately horizontal (outward to the right), and the vertical direction approximately poloidal (downward in the ion grad-B drift direction). The Dα light emission is the vertical orange band just inside the separatrix, which is shown by the dashed white line. The projection of the RF antenna is shown by the dotted orange line, and the GPI gas manifold is shown by the vertical solid line. The vertical region used to evaluate the radial profile of GPI emission is between the two horizontal red lines, and the small black 1.5 cm x 1.5 cm square 1 cm inside the separatrix is used to evaluate the turbulence. In part (b) is the GPI signal level *vs.* time and local major radius for this shot, along with the separatrix, shown as a black dashed line. The false-color relative Dα brightness level scale is at the right.

9. Time evolution of the Dα light emission for one of the shots in the first group in Table 1. Part (a) shows the time dependence of the GPI Dα light emission averaged over the whole GPI field of view. Part (b) shows the variation of GPI radial profiles over this time, averaged between the horizontal lines in Fig. 2 and plotted every 2.5 msec, with the relative time from earliest (black) to latest (red), following the color scale of Fig. 8(b). Part (c) shows the peak location (black) and full-width at half maximum (blue) of these GPI profiles with respect to the average local separatrix position at the GPI view (zero on this scale), and the separatrix position vs. time (red line with diamonds).

10. The GPI signal levels (a), peak locations (b) and widths (FWHM) of the Dα light emission (c) vs. time for six of the H-mode shots of Table 1, calculated in the same way as for Fig. 9 and plotted with respect to the peak time of the GPI emission signals. The vertical lines show beginning of the puff and its peak 20 msec later. There is no systematic time variation of the GPI peak location or width vs. time during the puff in these cases.

11. Part (a) shows the time dependence of the GPI signal within the small 1.5 cm square region shown in Fig. 8 centered 1 cm inside the average separatrix position over this time for this shot. Overlaid in orange is this same signal smoothed over 1 msec. Part (b) shows the frequency spectrum of the amplitude fluctuations in the normalized GPI signal in this region vs. time, i.e. of the signal divided by its value smoothed over 1 msec. The amplitude scale is shown by the color bar at the upper right.

12. Several turbulence quantities as a function of time for the same six H-mode shots used for Fig. 10, where the time is again measured with respect to the peak of the GPI signal level. Part (a) shows the GPI signal levels, part (b) shows the rms/mean, part (c) shows the autocorrelation times, parts (d) and (e) show the poloidal and radial correlation lengths, and part (f) shows the poloidal velocities. There are no significant variations in the edge turbulence vs. the time over the duration of these GPI puffs.

13. Several other diagnostic signals as a function of time across the GPI puff for the same shots as in Fig. 2(a), where one shot has no puff (#138843) and the three successive shots have a similar puff (top panel). Part (a) shows the GPI Dα signals, Part (b) shows the edge USXR signals, part (c) shows the separatrix locations, part (d) shows the divertor Dα signals, part (e) shows the total radiated power, and part (f) shows the neutron rates. In general, these signals are consistent with a relatively small effect of the GPI puff on both the edge and core plasma.

14. Edge ion temperature (a) and toroidal rotation speed (b) measured using passive visible spectroscopy of the CIII line, which is located just inside the separatrix. This analysis is plotted the same way as in Figs. 6 and 7, with the values before the puff on the horizontal axis and the values at three times after the start of the puff on the vertical axis. There is little or no systematic change in T_i or V_{tor} after the puff, although there is considerable shot-to-shot scatter. The lines show linear fits to the data.

15. Data from the beam emission spectroscopy (BES) diagnostic, which measures the Dα light emission from the NBI, showing an increase in BES signal level (a) and fluctuation level (b) at ~3 cm inside the separatrix, which correlate with the the GPI puff (d). This BES sightline is near the GPI gas puff cloud and its signal level is affected by the increased in neutral density. However, the RMS level of the fluctuations above 4 kHz normalized to the low pass filtered signal seen by this BES channel (c) is not affected by the GPI puff.

16. In part (a) are volumetric energy source rates from DEGAS 2 simulation of shot #138846 at the peak of the gas puff (0.615 sec), integrated over flux surfaces and mapped to major radius at midplane. The corresponding Dα emission rate is included for reference. In part (b) are the radial locations of simulated (blue) and experimental (red) emission peaks relative to the separatrix. The electron temperature at the separatrix is included for reference. The radial difference of ~2 cm between DEGAS 2 and GPI at 645 msec is relatively small (comparable to the Thomson spatial resolution), and most likely due to a random fluctuation in edge profiles.

17. Results from UEDGE modeling of shot #138846, showing the calculated response at the separatrix for a simulated GPI gas puff. The neutral gas density (n_g) closely follows the rise and fall of the gas puff rate, and the deuterium ion density (n_i) rises for 30 msec after the peak puff due to the recycling and divertor detachment in the simulation. As a consequence the ion and electron temperature decrease by a similar fraction, since the total energy in the edge plasma is nearly constant in this simulation.

References

[1] S.A. Sabbagh, J.-W. Ahn, J. Allain, R. Andre *et al*, Nucl. Fusion **53**, 014007 (2013)

[2] R.J. Maqueda, G.A. Wurden, D.P. Stotler *et al*, Rev. Sci. Inst. **74**, 2020 (2003)

[3] S. Zweben, R.J. Maqueda, D.P. Stotler *et al*, Nucl. Fusion **44**, 134 (2004)

[4] B. Cao, D.P. Stotler, S.J. Zweben *et al*, Fus. Sci. Tech. **64**, 29 (2013)

[5] M.A. Pedrosa, I. Garcia-Cortez, B. Franas *et al*, Phys. Plasmas **2**, 2618 (1995)

[6] P. Jacquet, V, Bobkov, M.-L. Mayoral *et al*, Nuc. Fusion **52**, 042002 (2012)

[7] A Ekedahl, V Petrzilka, Y. Baranov3, T.M. Biewer *et al*, Plasma Phys. Control. Fusion **54** 074004 (2012)

[8] R. Jha, A. Sen, P.K. Kaw *et al*, Plasma Phys. Control. Fusion **51,** 095010 (2009)

[9] D. Sangwan, R. Jha, J. Brotankova, and M. V. Gopalkrishna, Phys. Plasmas **20**, 062503 (2013);

[10] M Dreval, M Hubeny1, Y Ding, T Onchi *et al*, Plasma Phys. Control. Fusion **55** 035004 (2013)

[11] S. J. Zweben, D. P. Stotler, J. L. Terry, B. LaBombard *et al*, Phys. Plasmas **9**, 1981 (2002)

[12] S. J. Zweben , J. L. Terry , M. Agostini , W. M. Davis , A. Diallo et al. Phys. Plasmas **20**, 072503 (2013);

[13] S. C. Liu , L. M. Shao , S. J. Zweben , G. S. Xu , H. Y. Guo *et al,* Rev. Sci. Instrum. **83**, 123506 (2012);

[14] I. Shesterikov, Y. Xu, M. Berte, P. Dumortier, M. Van Schoor *et al,* Rev. Sci. Instrum. 84, 053501 (2013)

[15] R. Panek, J.P. Gunn, J. Bucalossi, I. Duran *et al*, J. Nucl. Mat. 337-339, 530 (2005)

[16] B. Unterberg, S. Brezinsek, G. Sergienko, C.C. Chu *et al*, J. Nucl. Mat. 337-339, 515 (2005)

[17] L. G. Askinazi , V. E. Golant , S. V. Lebedev , L. S. Levin , V. A. Rozhansky *et al,* Phys. Fluids **B 5**, 2420 (1993);

[18] A.R. Field, P.G. Carolan, N.J. Conway, G.F. Counsell *et al*, Plasma Phys. Control. Fusion **46** (2004) 981–1007

[19] R. Maingi, C.S. Chang, S. Ku, T. Biewer *et al*, Plasma Phys. Control. Fusion **46** (2004) A305–A313

[20] J.D. Strachan, N. Bretz, E. Mazzucato, C.W. Barnes *et al* Nucl. Fusion **22,** 1145 (1982)

[21] K. W. Gentle, B., Richards, F. Waelbroeck, Plasma Phys. Cont. Fusion 29, 1077 (1987)

[22] P. C. Efthimion, C. W. Barnes, M. G. Bell, H. Biglar *et al*, Phys. Fluids B **3**, 2315 (1991)

[23] D.R. Baker, M.R. Wade, G.L. Jackson, R. Maingi *et al*, Nucl. Fusion **38** 485 (1998)

[24] V.A. Vershkov, M.A. Borisov, G.F. Subbotin, D.A. Shelukhin *et al*, Nucl. Fusion **53** 083014 (2013)

[25] B. A. Carreras, L. W. Owen, R. Maingi , P. K. Mioduszewski *et al,* Phys. Plasmas **5**, 2623 (1998);

[26] A. Odblom, P. J. Catto, and S. I. Krasheninnikov, Phys. Plasmas **6**, 3239 (1999)

[27] P. Helander, T. Fulop, and P.J. Catto, Phys. Plasmas **10**, 4396 (2003)

[28] R. Singh, A. Rogister, and P. Kaw, Phys. Plasmas **11**, 129 (2004)

[29] K. Miki, P.H. Diamond, S.-H. Hahn, W.W. Xiao et al, Phys. Plasmas **20**, 082304 (2013)

[30] M.Z. Tokar, Nucl. Fusion **23**, 1395 (1983)

[31] M.Z. Tokar, Plasma Phys. Cont. Fusion **35**, 119 (1993)

[32] M.Z. Tokar and M. Koltunov, Plasma Phys. Cont. Fusion **55**, 045013 (2013)

[33] M.Z. Tokar and M. Koltunov, Phys. Plasmas **20**, 102502 (2013)

[34] V. Petrzilka, J. Mailloux, J. Ongena et al, Plasma Phys. Control. Fusion **54**, 074005 (2012)

[35] G.D. Porter, T.W. Petrie, T.D. Rognlien, M.E. Rensink, Phys. Plasmas **17**, 112501 (2010)

[36] V. A. Soukhanovskii , H. W. Kugel , R. Kaita , R. Majeski , and A. L. Roquemore Rev. Sci. Instrum. 75, 4320 (2004);

[37] L. R. Baylor , N. Commaux , T. C. Jernigan , S. J. Meitner , S. K. Combs et al. Phys. Plasmas 20, 082513 (2013)

[38] G.P. Maddison, C. Giroud, G.K. McCormick, B. Alper *et al*, Nucl. Fusion **51,** 082001 (2011)

[39] E.H. Hollman, T.C. Jernigan, M. Groth, M et al, Nucl. Fusion **45**, 1046 (2005)

[40] G.M. Olynyk, R.S. Granetz, M.L. Reinke, D.G. Whyte *et al*, Nucl.Fusion **53,** 092001 (2013)

[41] V.A. Soukhanovskii, R.E. Bell, C. Bush, R. Kaita et al, J. Nucl. Mat. **390-391**, 516 (2009)

[42] S.J. Zweben, B. D. Scott, J. L. Terry, B. LaBombard *et al*, Phys. Plasmas **16**, 082505 (2009)

[43] K. Tritz, D.J. Clayton, D. Stutman, et al, Rev. Sci. Inst. **83**, 10E109 (2012)

[44] T. M. Biewer, R. E. Bell, R. Feder, D. W. Johnson, and R. W. Palladino, Rev. Sci. Inst. **75**, 650 (2004)

[45] Y. Sechrest et al, to be submitted

[46] S.J. Zweben, R. J. Maqueda, R. Hager, K. Hallatschek *et al*, Phys. Plasmas **17**, 102502 (2010)

[47] Y. Sechrest, T. Munsat, D.J. Battaglia and S.J. Zweben, Nucl. Fusion 52, 123009 (2012)

[48] R.J. Maqueda, R. Maingi and NSTX Team, Phys. Plasmas **16,** 056117 (2009)

[49] V.A. Soukhanovskii, R. Maingi, R. Raman, H.W. Kugel *et al*, J. Nucl. Mat **313-316**, 573 (2003)

[50] D. P. Stotler, J. Boedo, B. LeBlanc, R. J. Maqueda, and S. J. Zweben, J. Nucl. Mater. **363-365**, 686 (2007)

[51] T. D. Rognlien, J. L. Milovich, M. E. Rensink, and G. D. Porter, J. Nucl. Mater. **196**, 347–351 (1992)

[52] S. I. Braginskii, In M. A. Leontovitch, editor, Rev. Plasma Phys., Vol. 1, pages 205–311. Consultants Bureau, New York, NY, 1965

[53] Y.P. Chen, Phys. Plasmas 18, 062506 (2011)

[54] J.M. Canik, R. Maingi et al Phys. Plasmas **18**, 056118 (2011)

[55] J.M. Canik, W. Guttenfelder, R. Maingi et al, Nucl. Fusion **53**, 113016 (2013)

[56] M. Agostini, P. Scarin, R. Cavazzana et al, Rev. Sci. Inst. 81, 10D715 (2010)

[57] E. de la Cal, J. Guasp and the TJ-II Team, Plasma Phys. Cont. Fusion 53, 085006 (2011)

[58] D.J. Battaglia, C.S. Chang, S.M. Kaye et al, Nucl. Fusion 53, 113032 (2013)

[59] J. Lang and C.S. Chang, neutral effects on edge turbulence, to be published

[60] C. Theiler, R.M. Churchill, B. Lipschultz et al, submitted to Nuclear Fusion (2014)

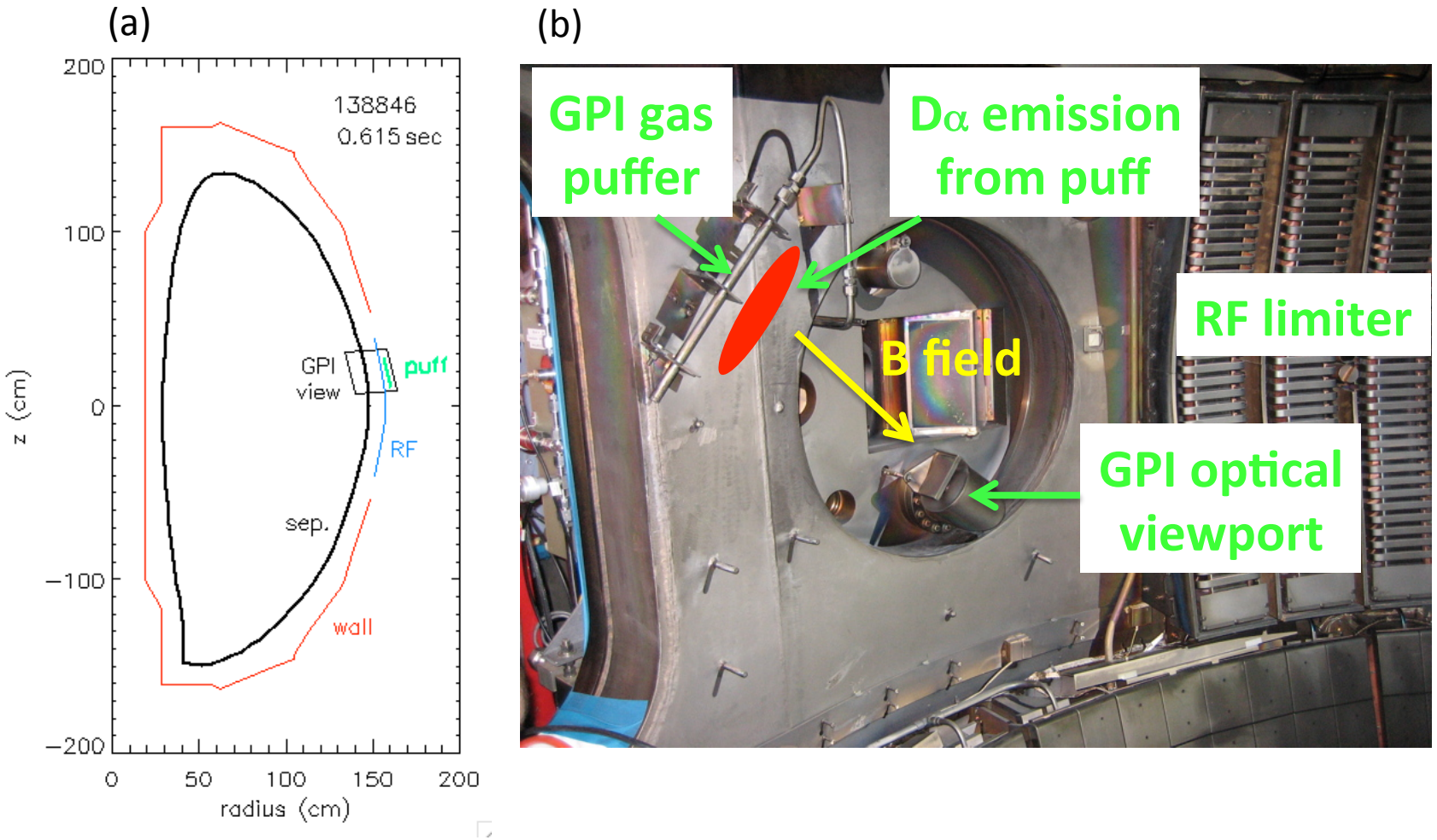
(a)
(b)
138846
0.615 sec
GPI
view
puff
RF
sep.
wall
z (cm)
radius (cm)
200
100
0
−100
−200
0
50
100
150
200
GPI gas puffer
Dα emission from puff
RF limiter
B field
GPI optical viewport

Fig. 1

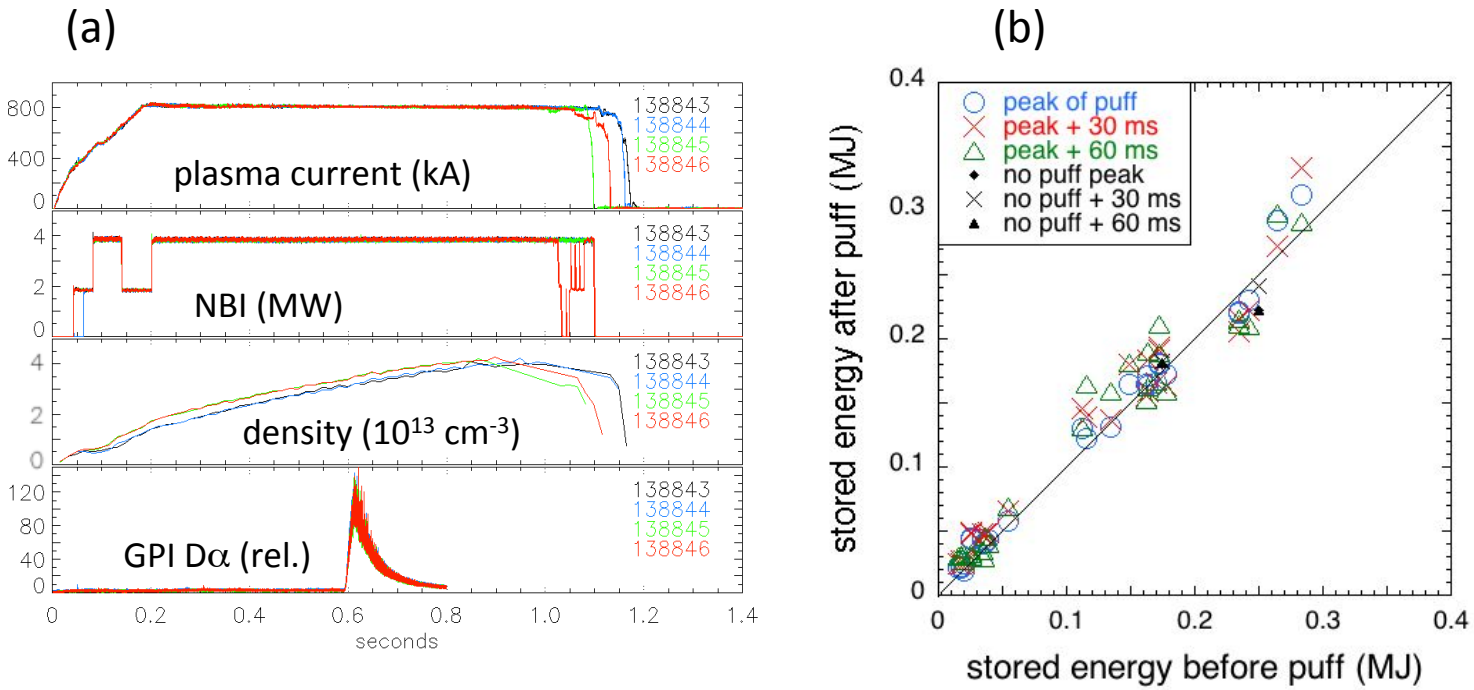
(a)
plasma current (kA)
NBI (MW)
density (10^{13} cm^{-3})
GPI Dα (rel.)
138843
138844
138845
138846
seconds
(b)
peak of puff
peak + 30 ms
peak + 60 ms
no puff peak
no puff + 30 ms
no puff + 60 ms
stored energy after puff (MJ)
stored energy before puff (MJ)

Fig. 2

(a)

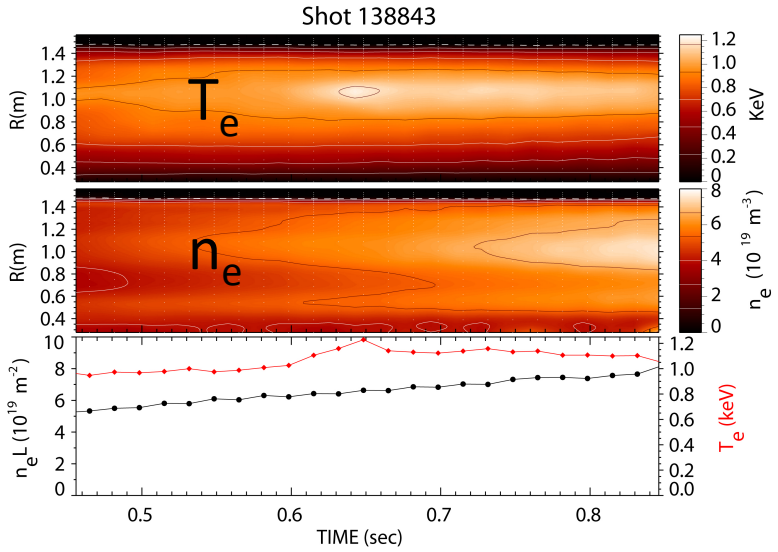
Shot 138843
T_e
n_e
R(m)
KeV
n_e (10^19 m^-3)
n_e L (10^19 m^-2)
T_e (keV)
TIME (sec)

(b)

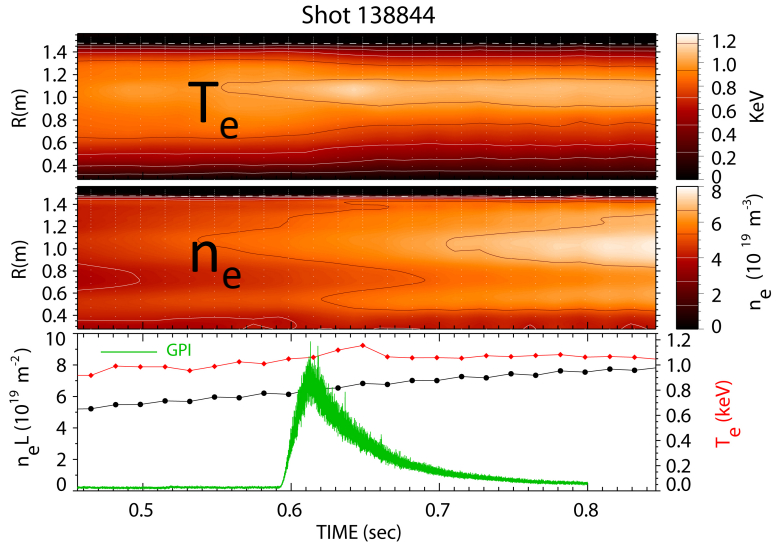
Shot 138844
T_e
n_e
R(m)
KeV
n_e (10^19 m^-3)
n_e L (10^19 m^-2)
GPI
T_e (keV)
TIME (sec)

Fig. 3

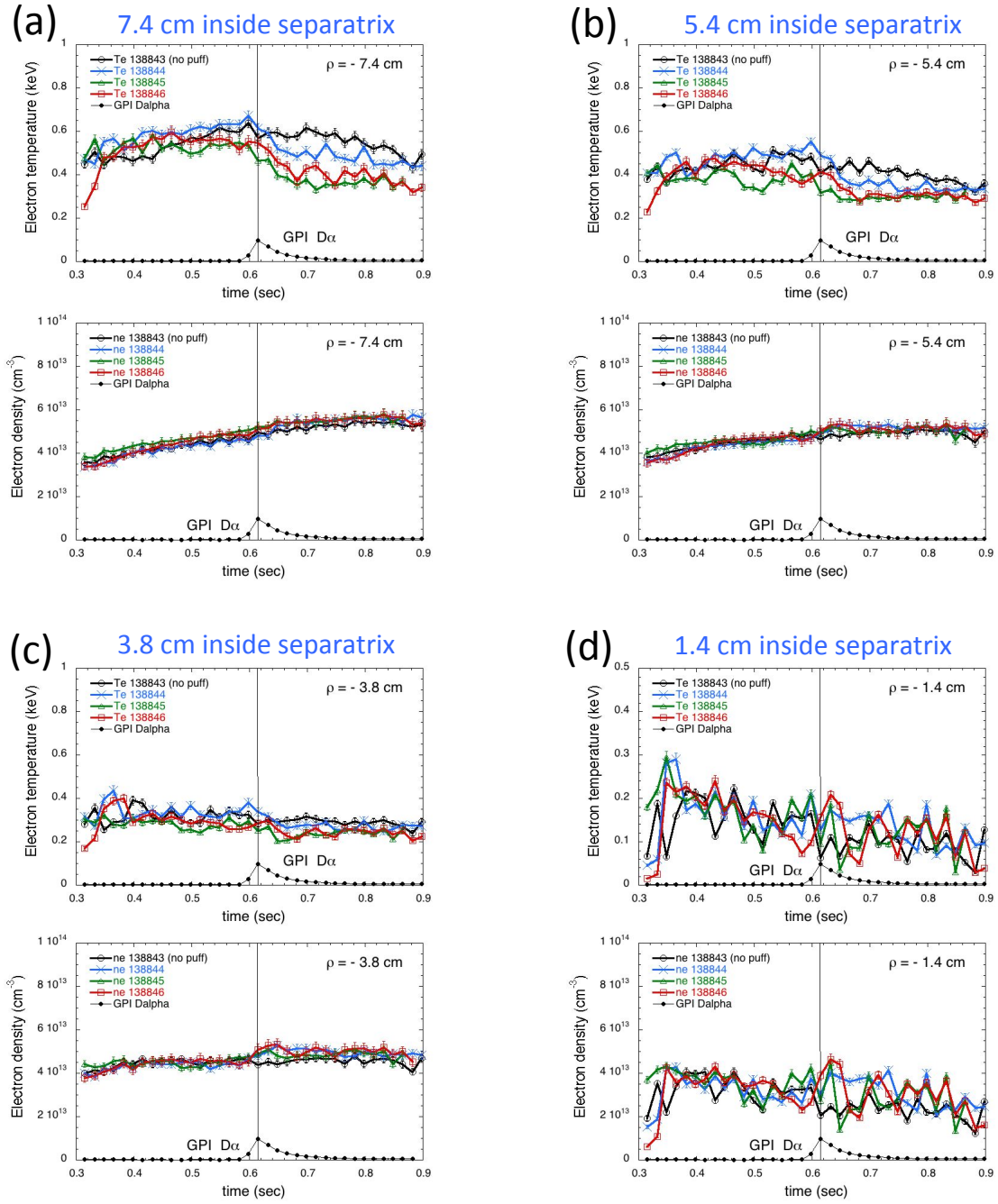
(a)
7.4 cm inside separatrix
(b)
5.4 cm inside separatrix
(c)
3.8 cm inside separatrix
(d)
1.4 cm inside separatrix
Te 138843 (no puff)
Te 138844
Te 138845
Te 138846
GPI Dalpha
ne 138843 (no puff)
ne 138844
ne 138845
ne 138846
ρ = - 7.4 cm
ρ = - 5.4 cm
ρ = - 3.8 cm
ρ = - 1.4 cm
GPI Dα
Electron temperature (keV)
Electron density (cm-3)
time (sec)

Fig. 4

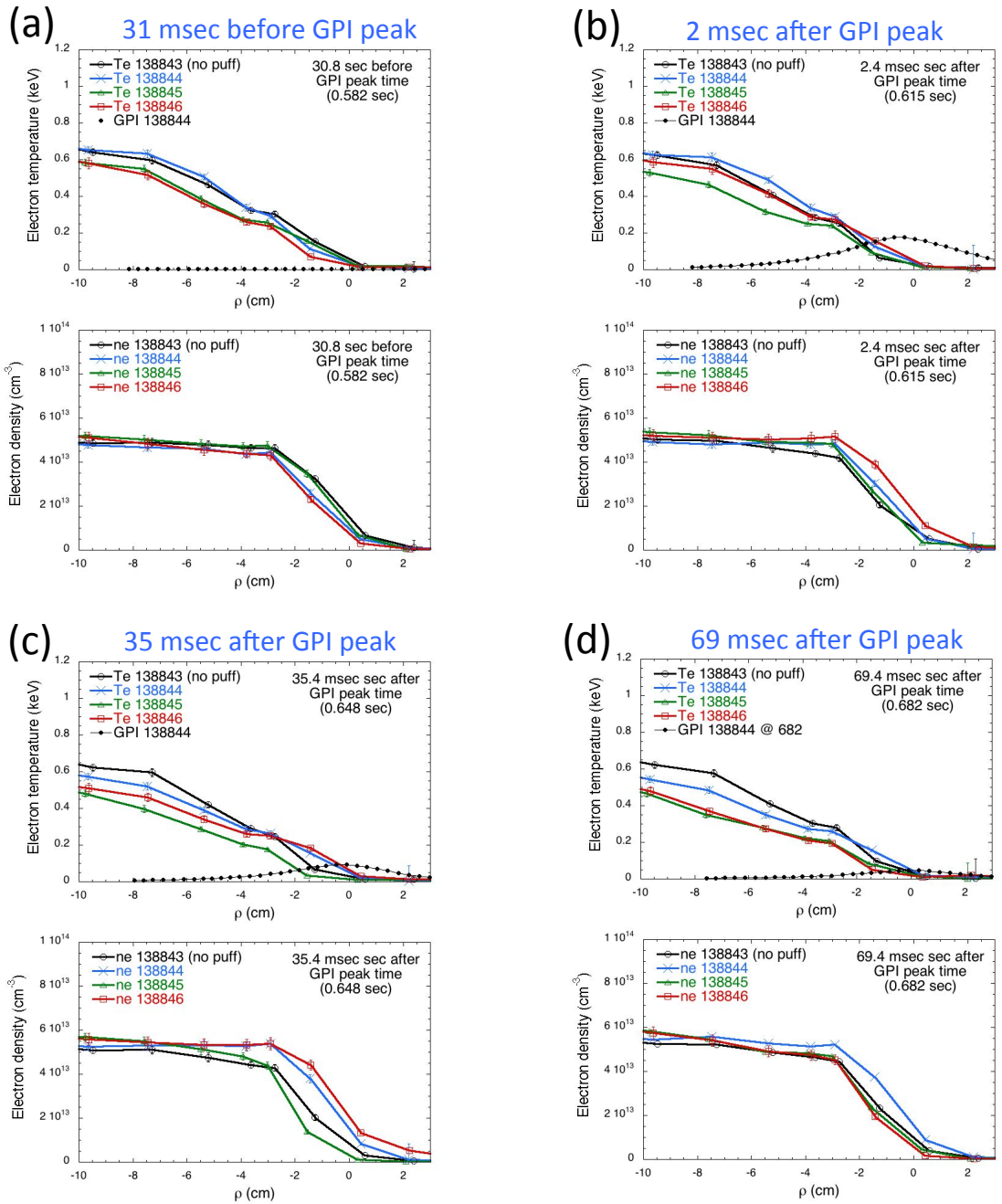
(a)
31 msec before GPI peak
Te 138843 (no puff)
Te 138844
Te 138845
Te 138846
GPI 138844
30.8 sec before GPI peak time (0.582 sec)
Electron temperature (keV)
ρ (cm)
ne 138843 (no puff)
ne 138844
ne 138845
ne 138846
Electron density (cm^{-3})
(b)
2 msec after GPI peak
2.4 msec sec after GPI peak time (0.615 sec)
(c)
35 msec after GPI peak
35.4 msec sec after GPI peak time (0.648 sec)
(d)
69 msec after GPI peak
GPI 138844 @ 682
69.4 msec sec after GPI peak time (0.682 sec)

Fig. 5

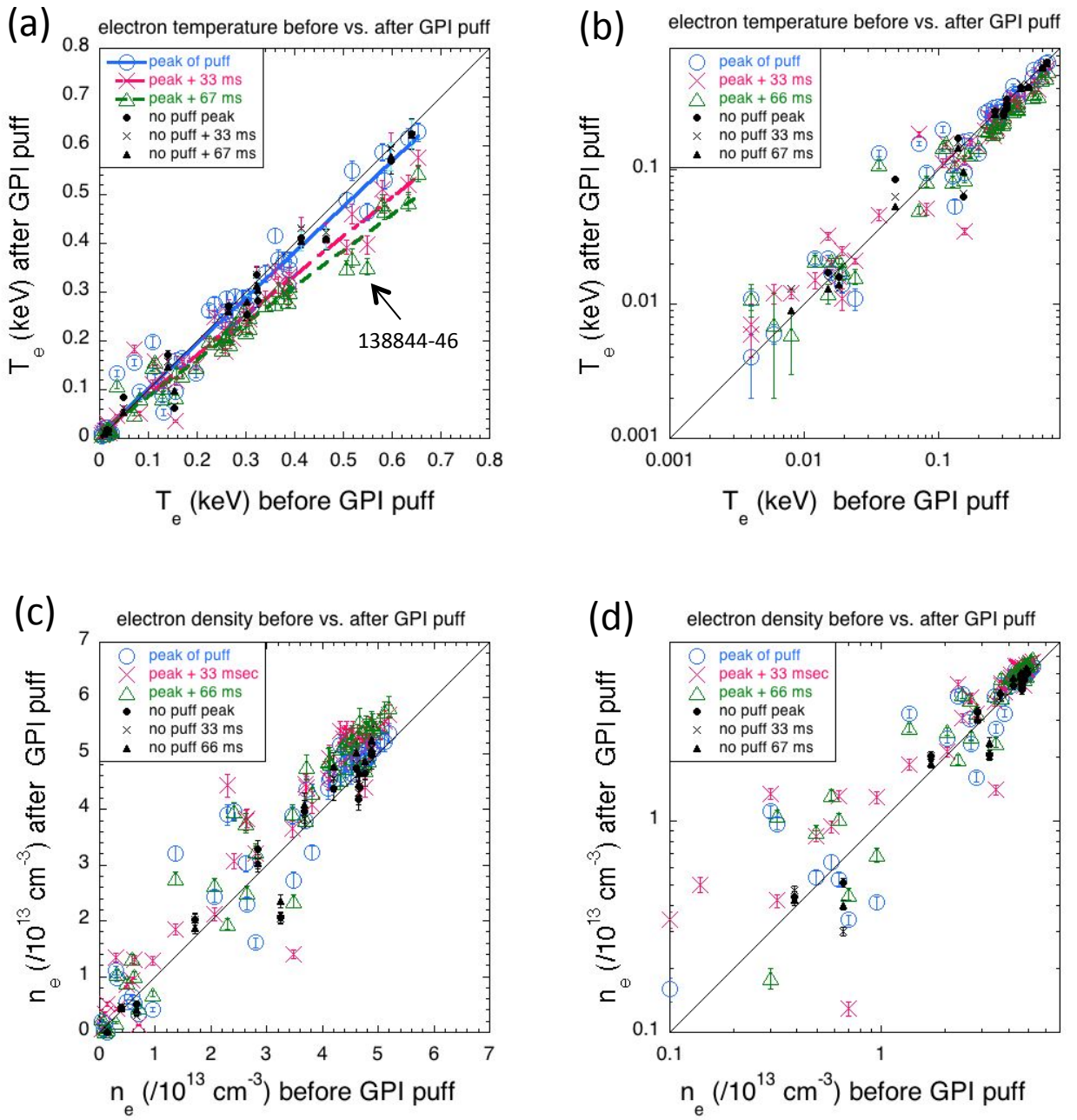
(a)
electron temperature before vs. after GPI puff
peak of puff
peak + 33 ms
peak + 67 ms
no puff peak
no puff + 33 ms
no puff + 67 ms
138844-46
T_e (keV) after GPI puff
T_e (keV) before GPI puff
(b)
electron temperature before vs. after GPI puff
peak of puff
peak + 33 ms
peak + 66 ms
no puff peak
no puff 33 ms
no puff 67 ms
T_e (keV) after GPI puff
T_e (keV) before GPI puff
(c)
electron density before vs. after GPI puff
peak of puff
peak + 33 msec
peak + 66 ms
no puff peak
no puff 33 ms
no puff 66 ms
n_e (/10^13 cm^-3) after GPI puff
n_e (/10^13 cm^-3) before GPI puff
(d)
electron density before vs. after GPI puff
peak of puff
peak + 33 msec
peak + 66 ms
no puff peak
no puff 33 ms
no puff 67 ms
n_e (/10^13 cm^-3) after GPI puff
n_e (/10^13 cm^-3) before GPI puff

Fig. 6

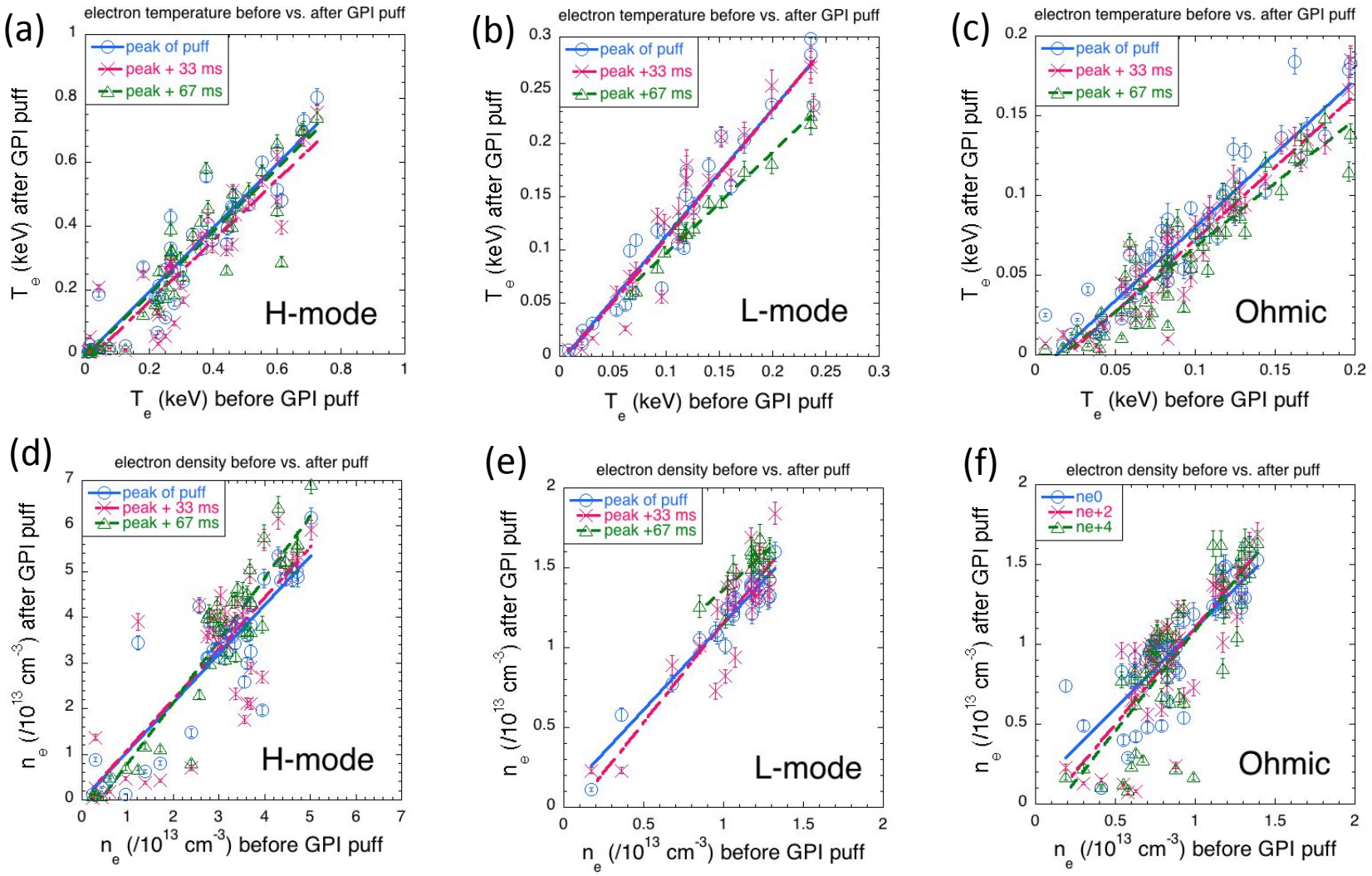
(a)
electron temperature before vs. after GPI puff
peak of puff
peak + 33 ms
peak + 67 ms
H-mode
T_e (keV) after GPI puff
T_e (keV) before GPI puff
(b)
electron temperature before vs. after GPI puff
peak of puff
peak +33 ms
peak +67 ms
L-mode
T_e (keV) after GPI puff
T_e (keV) before GPI puff
(c)
electron temperature before vs. after GPI puff
peak of puff
peak + 33 ms
peak + 67 ms
Ohmic
T_e (keV) after GPI puff
T_e (keV) before GPI puff
(d)
electron density before vs. after puff
peak of puff
peak + 33 ms
peak + 67 ms
H-mode
n_e (/10^13 cm^-3) after GPI puff
n_e (/10^13 cm^-3) before GPI puff
(e)
electron density before vs. after puff
peak of puff
peak +33 ms
peak +67 ms
L-mode
n_e (/10^13 cm^-3) after GPI puff
n_e (/10^13 cm^-3) before GPI puff
(f)
electron density before vs. after puff
ne0
ne+2
ne+4
Ohmic
n_e (/10^13 cm^-3) after GPI puff
n_e (/10^13 cm^-3) before GPI puff

Fig. 7

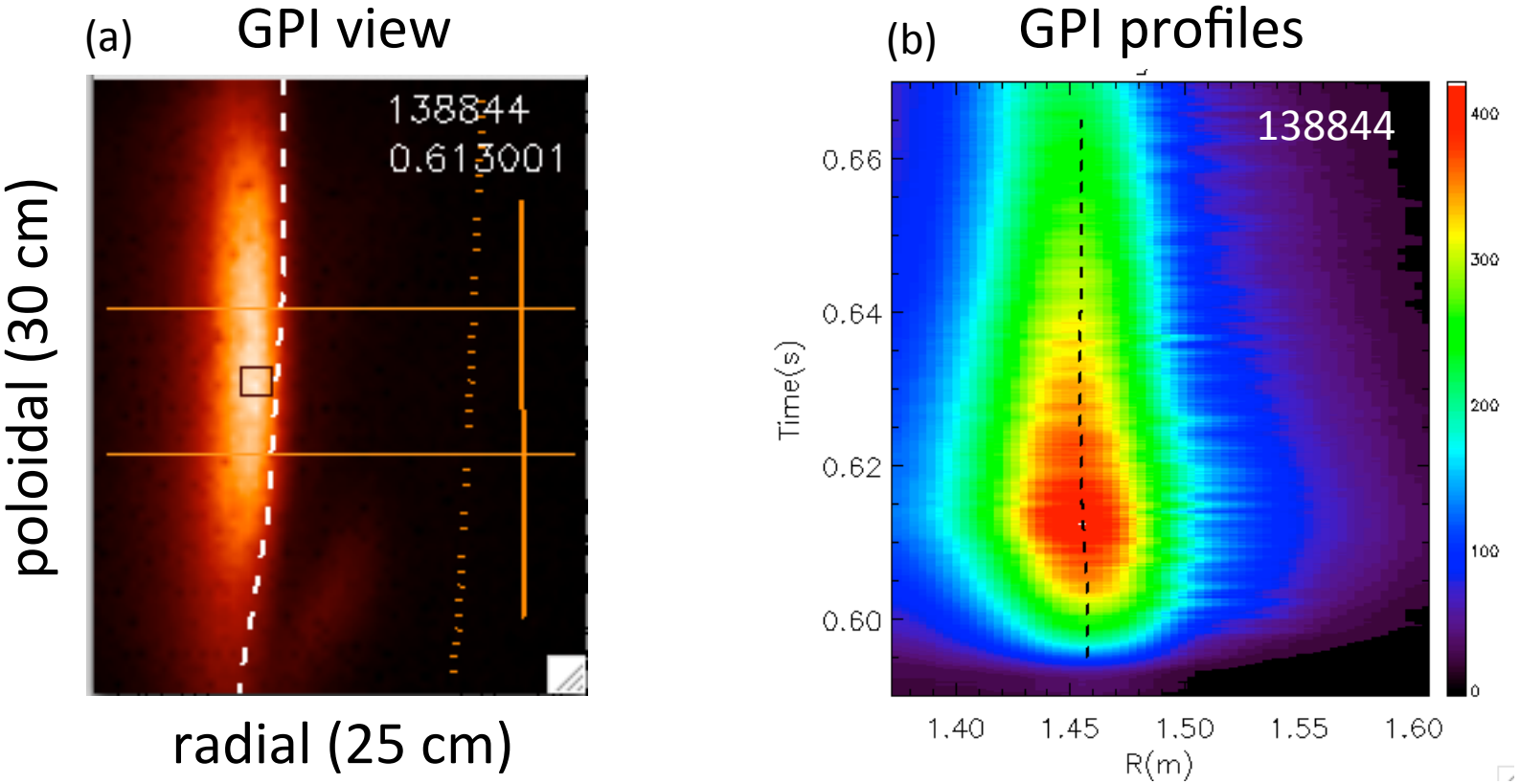
(a)
GPI view
138844
0.613001
poloidal (30 cm)
radial (25 cm)
(b)
GPI profiles
138844
0.66
0.64
0.62
0.60
Time(s)
1.40
1.45
1.50
1.55
1.60
R(m)
400
300
200
100
0

Fig. 8

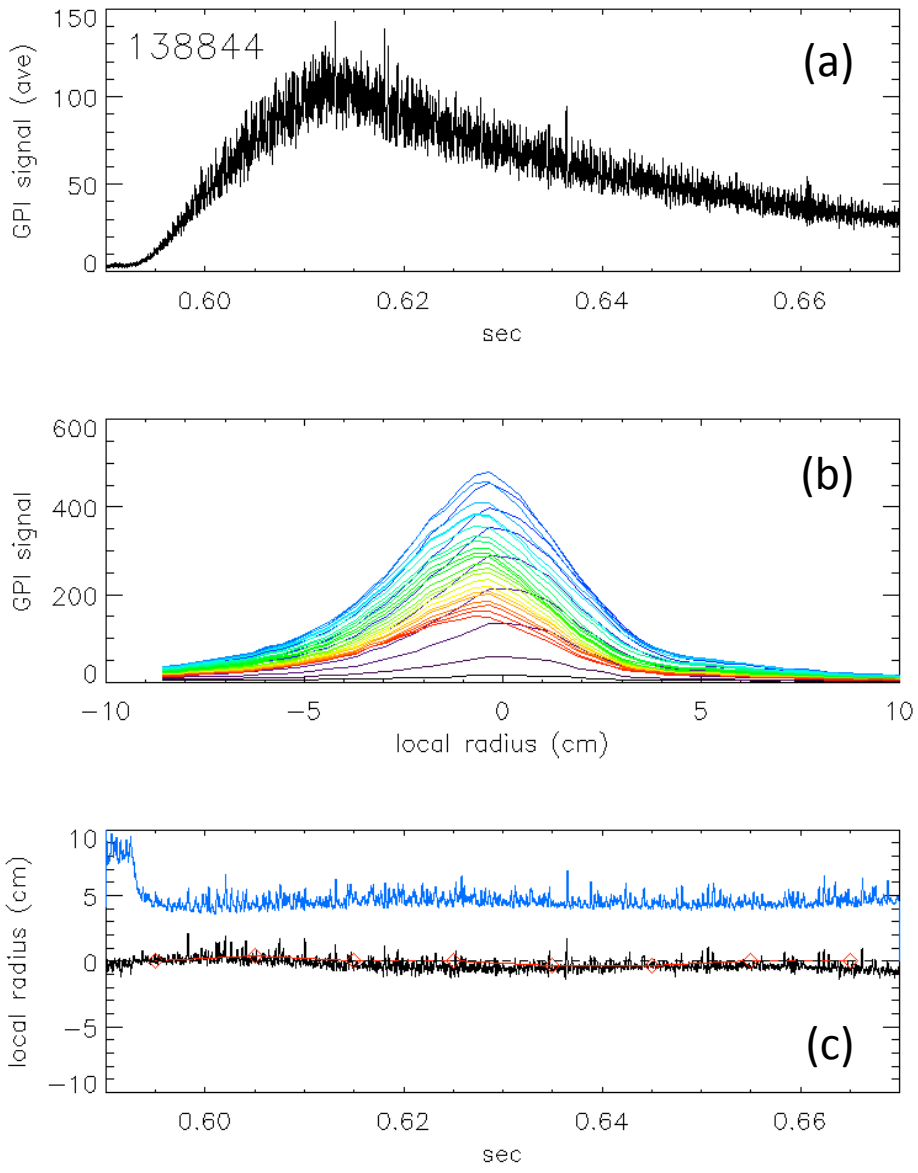
138844
(a)
GPI signal (ave)
150
100
50
0
0.60
0.62
0.64
0.66
sec
(b)
GPI signal
600
400
200
0
−10
−5
0
5
10
local radius (cm)
(c)
local radius (cm)
10
5
0
−5
−10
0.60
0.62
0.64
0.66
sec

Fig. 9

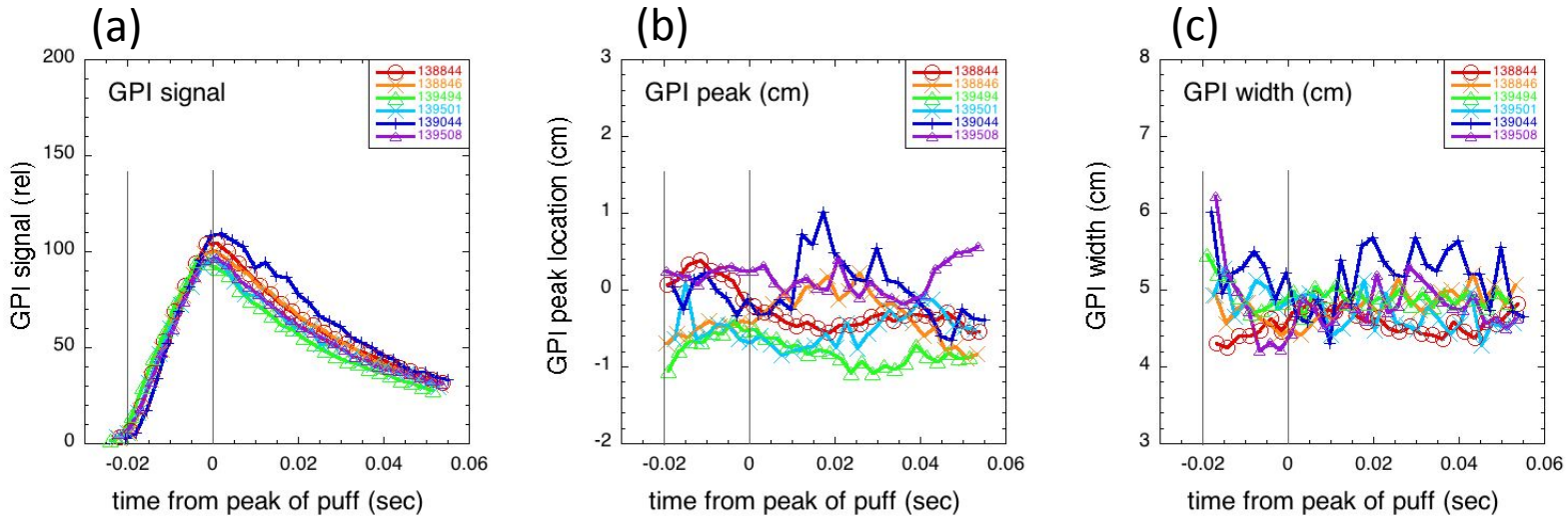
(a)
GPI signal
GPI signal (rel)
time from peak of puff (sec)
(b)
GPI peak (cm)
GPI peak location (cm)
time from peak of puff (sec)
(c)
GPI width (cm)
GPI width (cm)
time from peak of puff (sec)
138844
138846
139494
139501
139044
139508

Fig. 10

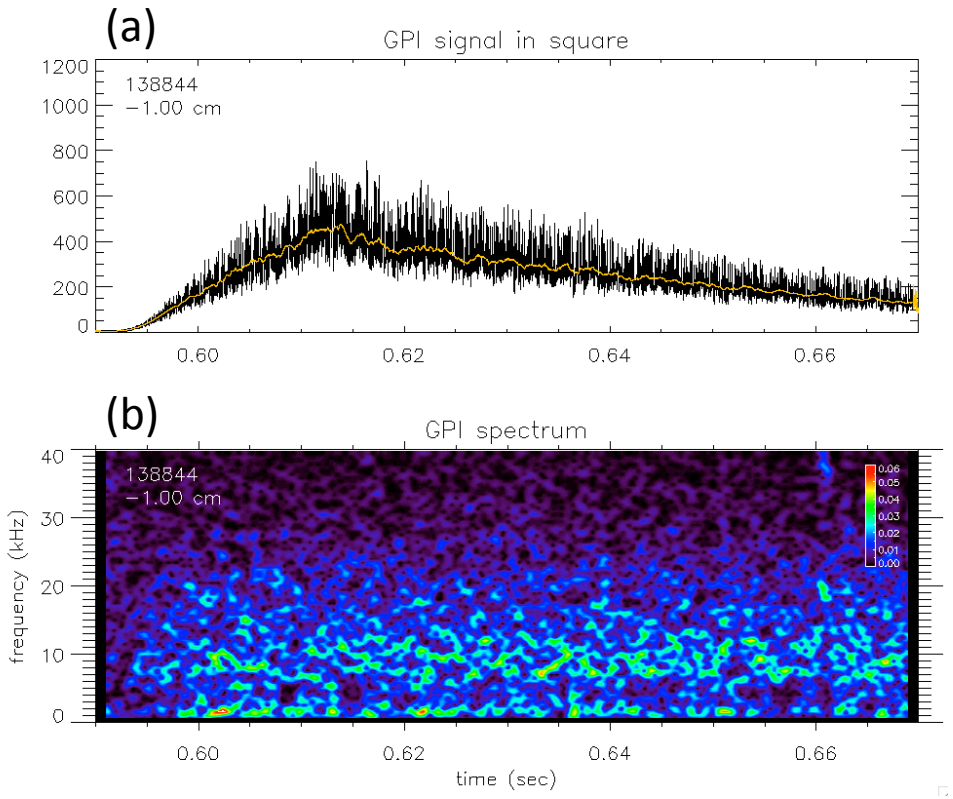
(a)
GPI signal in square
138844
−1.00 cm
1200
1000
800
600
400
200
0
0.60
0.62
0.64
0.66
(b)
GPI spectrum
138844
−1.00 cm
frequency (kHz)
40
30
20
10
0
0.60
0.62
0.64
0.66
time (sec)

Fig. 11

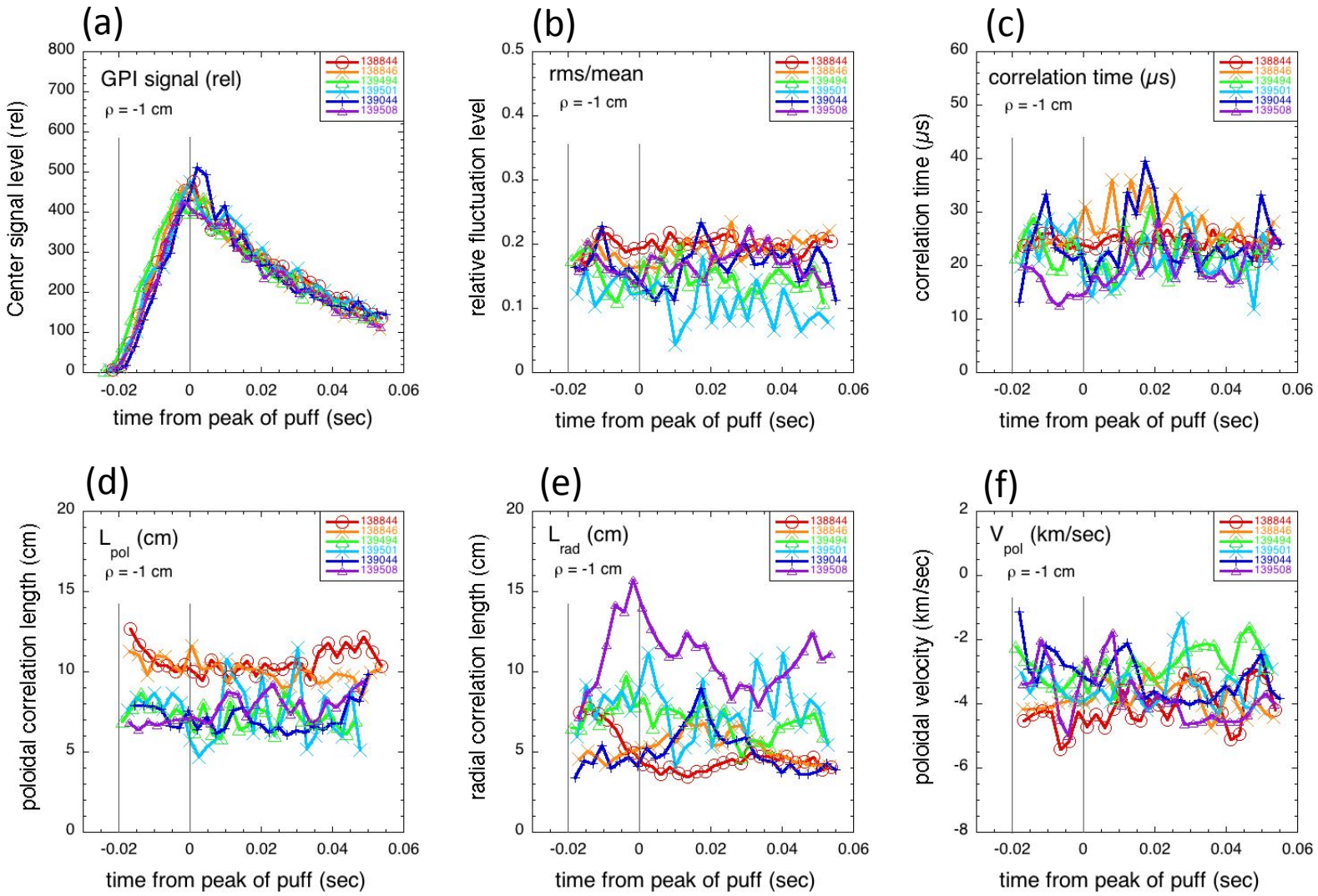
(a)
GPI signal (rel)
ρ = -1 cm
Center signal level (rel)
time from peak of puff (sec)
(b)
rms/mean
ρ = -1 cm
relative fluctuation level
time from peak of puff (sec)
(c)
correlation time (μs)
ρ = -1 cm
correlation time (μs)
time from peak of puff (sec)
(d)
L pol (cm)
ρ = -1 cm
poloidal correlation length (cm)
time from peak of puff (sec)
(e)
L rad (cm)
ρ = -1 cm
radial correlation length (cm)
time from peak of puff (sec)
(f)
V pol (km/sec)
ρ = -1 cm
poloidal velocity (km/sec)
time from peak of puff (sec)
138844
138846
139494
139501
139044
139508

Fig. 12

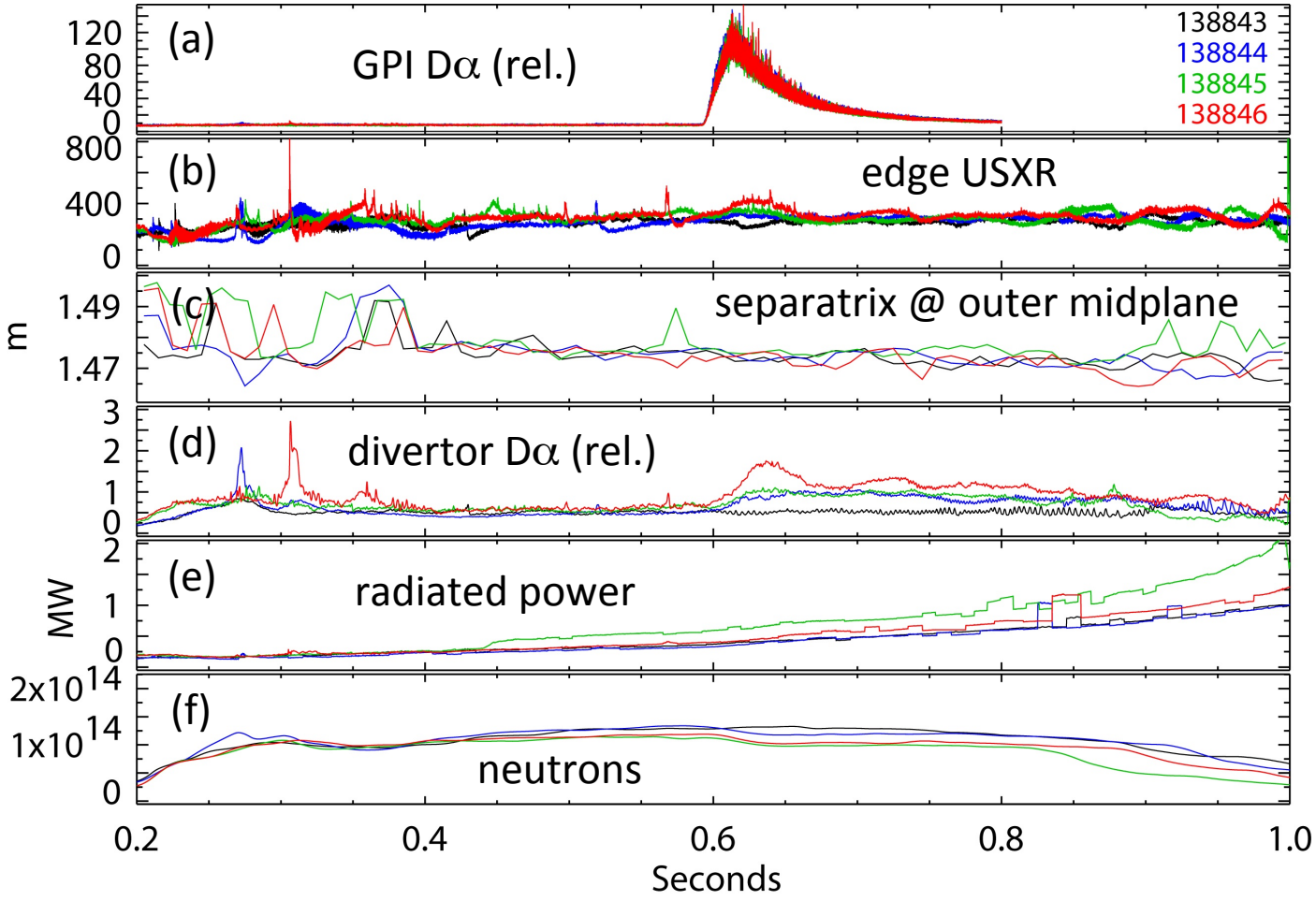
(a)
GPI Dα (rel.)
138843
138844
138845
138846
120
80
40
0
(b)
edge USXR
800
400
0
(c)
separatrix @ outer midplane
m
1.49
1.47
(d)
divertor Dα (rel.)
3
2
1
0
(e)
radiated power
MW
2
1
0
(f)
neutrons
2x10^14
1x10^14
0
0.2
0.4
0.6
0.8
1.0
Seconds

Fig. 13

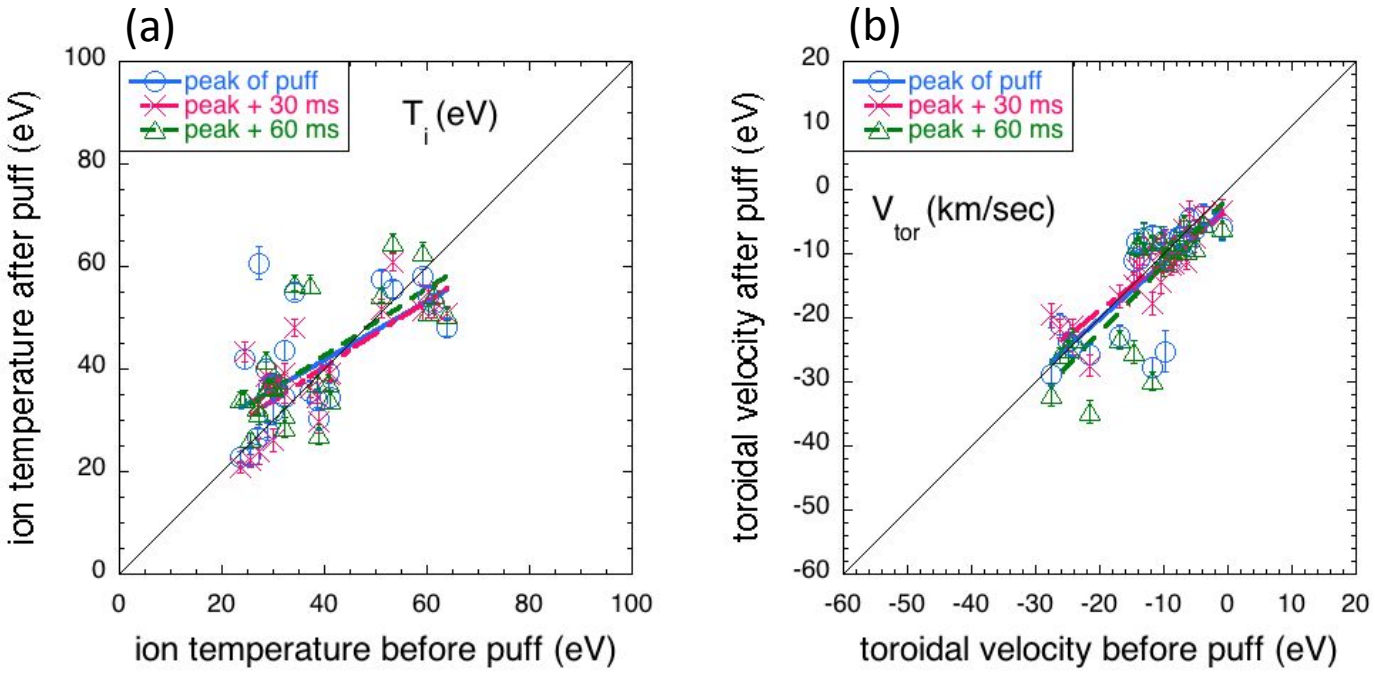
(a)
peak of puff
peak + 30 ms
peak + 60 ms
T_i (eV)
ion temperature after puff (eV)
ion temperature before puff (eV)
0
20
40
60
80
100
(b)
peak of puff
peak + 30 ms
peak + 60 ms
V_tor (km/sec)
toroidal velocity after puff (eV)
toroidal velocity before puff (eV)
-60
-50
-40
-30
-20
-10
0
10
20

Fig. 14

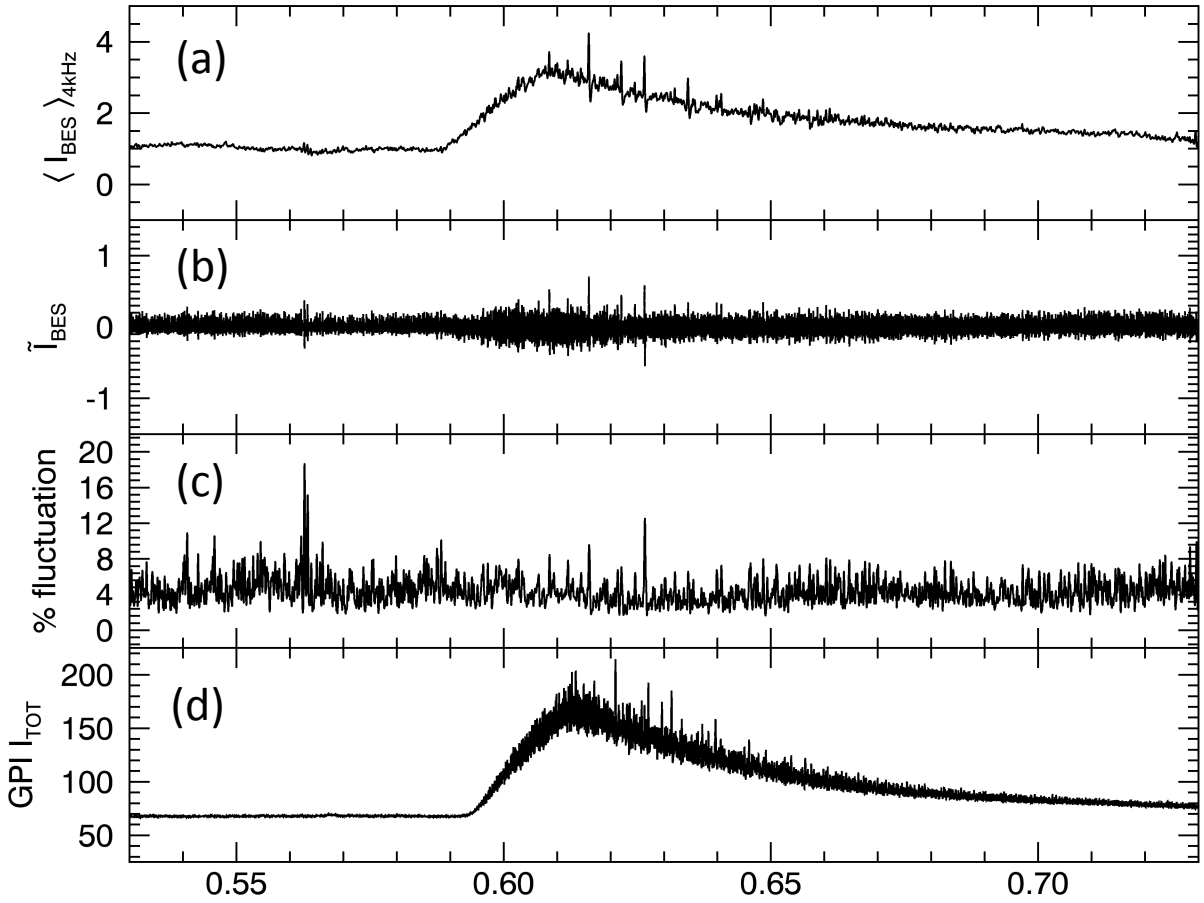
(a)
(b)
(c)
(d)
$\langle I_{BES} \rangle_{4kHz}$
$\tilde{I}_{BES}$
% fluctuation
GPI I_{TOT}
4
2
0
1
0
-1
20
16
12
8
4
0
200
150
100
50
0.55
0.60
0.65
0.70

Fig. 15

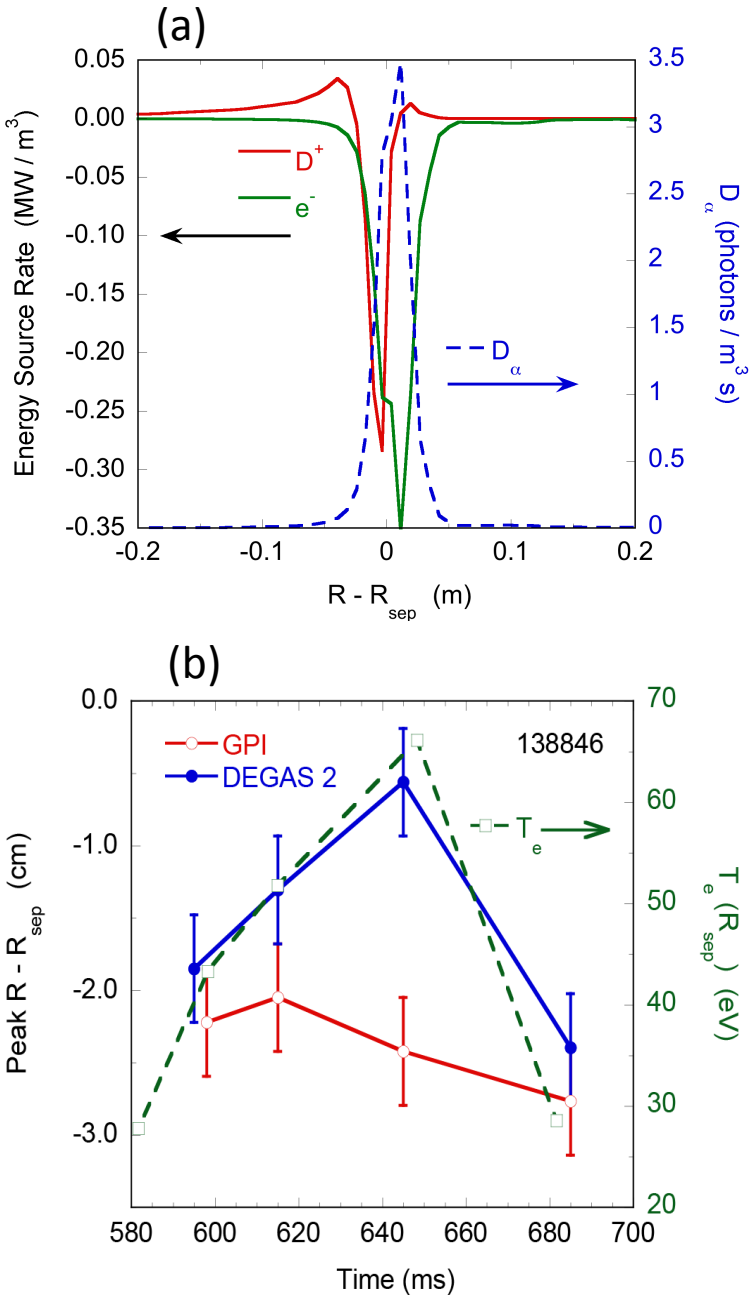
(a)
Energy Source Rate (MW / m3)
D+
e-
Dα
Dα (photons / m3 s)
R - Rsep (m)
(b)
GPI
DEGAS 2
138846
Te
Peak R - Rsep (cm)
Te (Rsep) (eV)
Time (ms)

Fig. 16

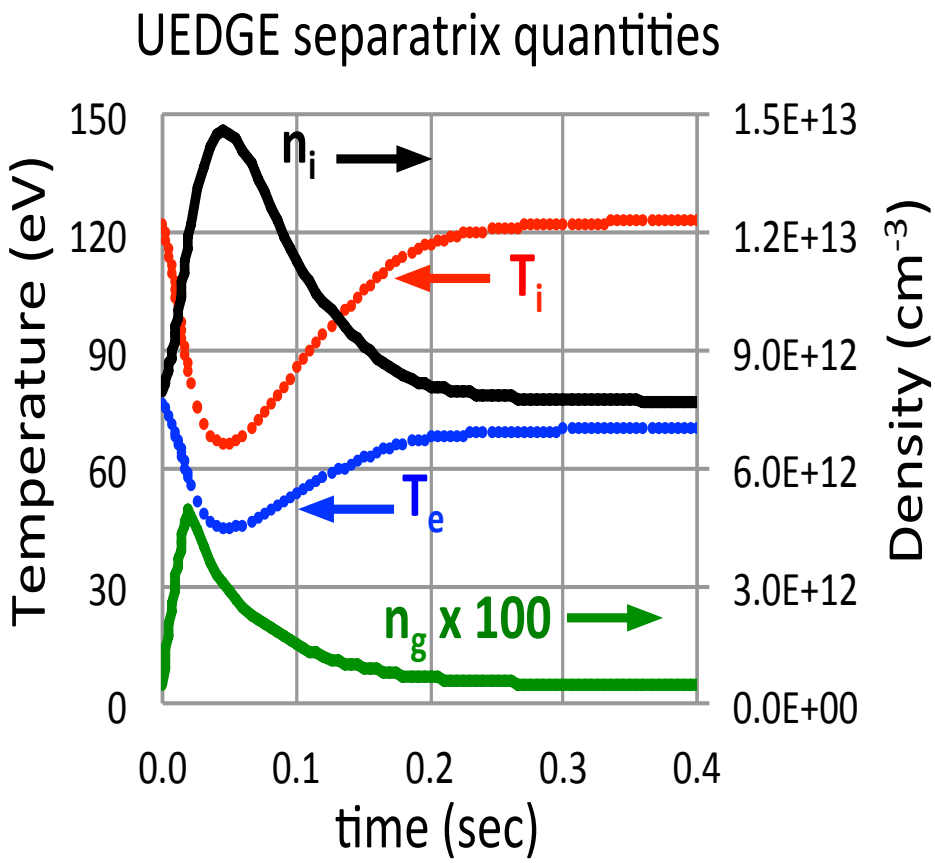
UEDGE separatrix quantities
Temperature (eV)
Density (cm-3)
time (sec)
150
120
90
60
30
0
1.5E+13
1.2E+13
9.0E+12
6.0E+12
3.0E+12
0.0E+00
0.0
0.1
0.2
0.3
0.4
ni
Ti
Te
ng x 100

Fig. 17

The Princeton Plasma Physics Laboratory is operated
by Princeton University under contract
with the U.S. Department of Energy.

Information Services
Princeton Plasma Physics Laboratory
P.O. Box 451
Princeton, NJ 08543

Phone: 609-243-2245
Fax: 609-243-2751
e-mail: pppl_info@pppl.gov
Internet Address: http://www.pppl.gov